



**NAVAL  
POSTGRADUATE  
SCHOOL**

**MONTEREY, CALIFORNIA**

**THESIS**

**DERIVATION OF RIVER BATHYMETRY  
USING IMAGERY FROM UNMANNED AERIAL  
VEHICLES (UAV)**

by

Matthew Pawlenko

September 2011

Thesis Advisor:

Philip A. Durkee

Co-Advisor:

K. Todd Holland

**Approved for public release; distribution is unlimited**

THIS PAGE INTENTIONALLY LEFT BLANK

<b>REPORT DOCUMENTATION PAGE</b>			<i>Form Approved OMB No. 0704-0188</i>
Public reporting burden for this collection of information is estimated to average 1 hour per response, including the time for reviewing instruction, searching existing data sources, gathering and maintaining the data needed, and completing and reviewing the collection of information. Send comments regarding this burden estimate or any other aspect of this collection of information, including suggestions for reducing this burden, to Washington headquarters Services, Directorate for Information Operations and Reports, 1215 Jefferson Davis Highway, Suite 1204, Arlington, VA 22202-4302, and to the Office of Management and Budget, Paperwork Reduction Project (0704-0188) Washington DC 20503.			
<b>1. AGENCY USE ONLY (Leave blank)</b>	<b>2. REPORT DATE</b> September 2011	<b>3. REPORT TYPE AND DATES COVERED</b> Master's Thesis	
<b>4. TITLE AND SUBTITLE</b> Derivation of River Bathymetry Using Imagery from Unmanned Aerial Vehicles (UAV)		<b>5. FUNDING NUMBERS</b>	
<b>6. AUTHOR(S)</b> Matthew Pawlenko		<b>8. PERFORMING ORGANIZATION REPORT NUMBER</b>	
<b>7. PERFORMING ORGANIZATION NAME(S) AND ADDRESS(ES)</b> Naval Postgraduate School Monterey, CA 93943-5000		<b>10. SPONSORING/MONITORING AGENCY REPORT NUMBER</b>	
<b>9. SPONSORING /MONITORING AGENCY NAME(S) AND ADDRESS(ES)</b> N/A		<b>11. SUPPLEMENTARY NOTES</b> The views expressed in this thesis are those of the author and do not reflect the official policy or position of the Department of Defense or the U.S. Government. IRB Protocol Number: N/A.	
<b>12a. DISTRIBUTION / AVAILABILITY STATEMENT</b> Approved for public release; distribution is unlimited		<b>12b. DISTRIBUTION CODE</b>	
<b>13. ABSTRACT (maximum 200 words)</b>  In many places that U.S. forces operate, there exists an insufficient amount of data regarding river water depths, which is a necessity for safe operational planning. Satellite sensors and airborne manned platforms have been used for bathymetric derivation, but are not in abundance, nor do they have the spatial resolution required to examine smaller rivers. Using Unmanned Aerial Vehicles (UAV), this research examines the feasibility of using a ratio method with digital imagery to derive water depths, as well as a simpler polynomial regression to create a lookup table for use in the field. The results show that the ratio method of Red to Blue had higher correlation than Red color band on its own, and that the simple polynomial regression using a ratio of Red to Blue had higher correlation than more widely accepted methods. However, both methods are limited by a maximum depth, which is defined as the point where color no longer changes with depth. All depths beyond this point appear as this maximum depth. These findings show that using imagery from UAVs for bathymetric derivation could be a feasible alternative to accepted satellite imagery methods, but further research is needed to demonstrate operational utility.			
<b>14. SUBJECT TERMS</b> Unmanned Aerial Vehicle, River Bathymetry, Remote Sensing, Bathymetric Derivation, Look-up Table, Beer's Law, Kootenai River, Trinity River		<b>15. NUMBER OF PAGES</b> 85	<b>16. PRICE CODE</b>
<b>17. SECURITY CLASSIFICATION OF REPORT</b> Unclassified	<b>18. SECURITY CLASSIFICATION OF THIS PAGE</b> Unclassified	<b>19. SECURITY CLASSIFICATION OF ABSTRACT</b> Unclassified	<b>20. LIMITATION OF ABSTRACT</b> UU

THIS PAGE INTENTIONALLY LEFT BLANK

**Approved for public release; distribution is unlimited**

**DERIVATION OF RIVER BATHYMETRY USING IMAGERY  
FROM UNMANNED AERIAL VEHICLES (UAV)**

Matthew Pawlenko  
Lieutenant Commander, United States Navy  
B.S., Purdue University, 2002

Submitted in partial fulfillment of the  
requirements for the degree of

**MASTER OF SCIENCE IN METEOROLOGY AND PHYSICAL  
OCEANOGRAPHY**

from the

**NAVAL POSTGRADUATE SCHOOL  
September 2011**

Author: Matthew Pawlenko

Approved by: Philip A. Durkee  
Thesis Advisor

K. Todd Holland  
Co-Advisor

Philip A. Durkee  
Dean, Graduate School of Engineering and Science

THIS PAGE INTENTIONALLY LEFT BLANK

## **ABSTRACT**

In many places that U.S. forces operate, there exists an insufficient amount of data regarding river water depths, which is a necessity for safe operational planning. Satellite sensors and airborne manned platforms have been used for bathymetric derivation, but are not in abundance, nor do they have the spatial resolution required to examine smaller rivers. Using Unmanned Aerial Vehicles (UAV), this research examines the feasibility of using a ratio method with digital imagery to derive water depths, as well as a simpler polynomial regression to create a lookup table for use in the field. The results show that the ratio method of Red to Blue had higher correlation than Red color band on its own, and that the simple polynomial regression using a ratio of Red to Blue had higher correlation than more widely accepted methods. However, both methods are limited by a maximum depth, which is defined as the point where color no longer changes with depth. All depths beyond this point appear as this maximum depth. These findings show that using imagery from UAVs for bathymetric derivation could be a feasible alternative to accepted satellite imagery methods, but further research is needed to demonstrate operational utility.

THIS PAGE INTENTIONALLY LEFT BLANK

# TABLE OF CONTENTS

<b>I.</b>	<b>INTRODUCTION.....</b>	<b>1</b>
<b>II.</b>	<b>BACKGROUND .....</b>	<b>5</b>
	<b>A. RADIATIVE TRANSFER FUNDAMENTALS .....</b>	<b>5</b>
	1. Electromagnetic Theory and Radiative Transfer .....	5
	2. Relating Radiance to Digital Numbers (DN) .....	7
	<b>B. UAV ISSUES .....</b>	<b>8</b>
	1. Imagery Collection.....	8
	2. Flight Issues .....	9
	<b>C. TEST SITES.....</b>	<b>9</b>
	1. Kootenai River, Bonners Ferry, Idaho .....	9
	2. Trinity River, Junction City, California .....	11
	3. Ground-Truth (Bathymetry Data) .....	13
	<b>D. METHODS .....</b>	<b>14</b>
	1. Beer-Lambert-Bouguer Law.....	14
	a. <i>The Equation</i> .....	14
	b. <i>Band Selection</i> .....	16
	2. Look-up Table (LUT) via Polynomial Regression .....	17
<b>III.</b>	<b>METHODOLOGY .....</b>	<b>21</b>
	<b>A. IMAGE CORRECTION .....</b>	<b>21</b>
	1. Kootenai River .....	21
	2. Trinity River .....	22
	<b>B. REGION OF INTEREST (ROI) SELECTION.....</b>	<b>22</b>
	1. Kootenai River .....	22
	2. Trinity River .....	23
	<b>C. DEPTH DERIVATIONS .....</b>	<b>24</b>
	1. Beer’s Law .....	24
	a. <i>Kootenai River</i> .....	24
	b. <i>Trinity River</i> .....	25
	2. LUT via Polynomial Regression .....	25
	a. <i>Kootenai River</i> .....	25
	b. <i>Trinity River</i> .....	26
<b>IV.</b>	<b>RESULTS .....</b>	<b>27</b>
	<b>A. BEER’S LAW.....</b>	<b>28</b>
	1. Kootenai River .....	28
	a. <i>Central Section</i> .....	28
	b. <i>Eastern Section</i> .....	31
	c. <i>Western Section</i> .....	34
	2. Trinity River .....	37
	a. <i>Sheridan Bar</i> .....	37
	b. <i>Chapman Ranch</i> .....	39
	<b>B. LOOKUP TABLE VIA POLYNOMIAL REGRESSION .....</b>	<b>41</b>

1.	<b>Kootenai River .....</b>	<b>41</b>
a.	<i>Central Section.....</i>	<i>41</i>
b.	<i>Eastern Section .....</i>	<i>44</i>
c.	<i>Western Section.....</i>	<i>46</i>
2.	<b>Trinity River.....</b>	<b>48</b>
a.	<i>Sheridan Bar .....</i>	<i>48</i>
b.	<i>Chapman Ranch .....</i>	<i>50</i>
<b>V.</b>	<b>DISCUSSION .....</b>	<b>51</b>
A.	<b>BEER'S LAW.....</b>	<b>51</b>
B.	<b>LUT VIA POLYNOMIAL REGRESSION.....</b>	<b>55</b>
<b>VI.</b>	<b>CONCLUSION .....</b>	<b>61</b>
A.	<b>METHODOLOGY .....</b>	<b>61</b>
B.	<b>OPERATIONAL FEASIBILITY .....</b>	<b>61</b>
C.	<b>FUTURE RESEARCH.....</b>	<b>62</b>
	<b>LIST OF REFERENCES.....</b>	<b>65</b>
	<b>INITIAL DISTRIBUTION LIST .....</b>	<b>67</b>

## LIST OF FIGURES

Figure 1.	Visible light portion of electromagnetic spectrum (Image available from ScienceBuddies.org 2011) .....	5
Figure 2.	Radiative Transfer .....	6
Figure 3.	Kootenai River, Braided Reach .....	10
Figure 4.	Eastern Section of Braided Reach.....	10
Figure 5.	Central Section of Braided Reach.....	11
Figure 6.	Western Section of Braided Reach .....	11
Figure 7.	Trinity River, Sheridan Bar, Image 271143.....	12
Figure 8.	Trinity River, Chapman Ranch, Image 273138 .....	13
Figure 9.	<i>Red DN</i> values versus depth for Kootenai River, Central Section. Red line represents exponential curve for Beer's Law and Green line represents curve plotted using LUT via polynomial regression. Blue lines represent the bounds used to create polynomial coefficients for LUT.....	27
Figure 10.	<i>PWD</i> Calculated using <i>Blue</i> . Beer's Law, Kootenai River, Central Section ...	29
Figure 11.	<i>PWD</i> Calculated using <i>Green</i> . Beer's Law, Kootenai River, Central Section.....	29
Figure 12.	<i>PWD</i> Calculated using <i>Red/Green</i> . Beer's Law, Kootenai River, Central Section.....	30
Figure 13.	<i>PWD</i> Calculated using <i>Red</i> . Beer's Law, Kootenai River, Central Section ...	30
Figure 14.	<i>PWD</i> Calculated using <i>Red/Blue</i> . Beer's Law, Kootenai River, Central Section.....	31
Figure 15.	<i>PWD</i> Calculated using <i>Red</i> . Beer's Law, Kootenai River, Eastern Section ...	32
Figure 16.	<i>PWD</i> Calculated using <i>Green</i> . Beer's Law, Kootenai River, Eastern Section.....	33
Figure 17.	<i>PWD</i> Calculated using <i>Blue</i> . Beer's Law, Kootenai River, Eastern Section...33	33
Figure 18.	<i>PWD</i> Calculated using <i>Red/Green</i> . Beer's Law, Kootenai River, Eastern Section.....	34
Figure 19.	<i>PWD</i> Calculated using <i>Red/Blue</i> . Beer's Law, Kootenai River, Eastern Section.....	34
Figure 20.	<i>PWD</i> Calculated using <i>Red</i> . Beer's Law, Kootenai River, Western Section ..	35
Figure 21.	<i>PWD</i> Calculated using <i>Green</i> . Beer's Law, Kootenai River, Western Section.....	36
Figure 22.	<i>PWD</i> Calculated using <i>Blue</i> . Beer's Law, Kootenai River, Western Section.....	36
Figure 23.	<i>PWD</i> Calculated using <i>Red/Green</i> . Beer's Law, Kootenai River, Western Section.....	37
Figure 24.	<i>PWD</i> Calculated using <i>Red/Blue</i> . Beer's Law, Kootenai River, Western Section.....	37
Figure 25.	<i>PWD</i> Calculated using <i>Red/Green</i> . Beer's Law, Trinity River, Sheridan Bar.....	38
Figure 26.	<i>PWD</i> Calculated using <i>Red/Blue</i> in Beer's Law, Trinity River, Sheridan Bar.....	39

Figure 27.	<i>PWD</i> Calculated using <i>Red</i> . Beer’s Law, Trinity River, Chapman Ranch.....	40
Figure 28.	<i>PWD</i> Calculated using <i>Red/Blue</i> . Beer’s Law, Trinity River, Chapman Ranch .....	40
Figure 29.	<i>PWD</i> Calculated using <i>Red/Green</i> in Beer’s Law, Trinity River, Chapman...	41
Figure 30.	Lookup Depth using <i>Blue</i> . Kootenai River, Central Section. ....	42
Figure 31.	Lookup Depth using <i>Red</i> . Kootenai River, Central Section .....	43
Figure 32.	Lookup Depth using <i>Green</i> . Kootenai River, Central Section .....	43
Figure 33.	Lookup Depth using <i>Red/Green</i> . Kootenai River, Central Section .....	44
Figure 34.	Lookup Depth using <i>Red/Blue</i> . Kootenai River, Central Section.....	44
Figure 35.	Lookup Depth using <i>Green</i> . Kootenai River, Eastern Section .....	45
Figure 36.	Lookup Depth using <i>Red</i> . Kootenai River, Eastern Section .....	46
Figure 37.	Lookup Depth using <i>Red/Blue</i> . Kootenai River, Eastern Section .....	46
Figure 38.	Lookup Depth using <i>Red/Green</i> . Kootenai River, Western Section .....	47
Figure 39.	Lookup Depth using <i>Red/Blue</i> . Kootenai River, Western Section .....	48
Figure 40.	Lookup Depth using <i>Red/Green</i> . Trinity River, Sheridan Bar .....	49
Figure 41.	Lookup Depth using <i>Red/Blue</i> , Trinity River, Sheridan Bar .....	49
Figure 42.	Lookup Depth using <i>Red/Blue</i> . Trinity River, Chapman Ranch .....	50
Figure 43.	Calculated using <i>Red</i> . Beer’s Law, Kootenai River, Eastern Section .....	52
Figure 44.	Calculated using <i>Red/Blue</i> in Beer’s Law, Kootenai River, Eastern Section..	52
Figure 45.	Calculated using <i>Red/Blue</i> . Beer’s Law, Trinity River, Sheridan Bar.....	54
Figure 46.	Lookup Depth using <i>Red/Blue</i> . Kootenai River, Eastern Section .....	56
Figure 47.	Lookup Depth using <i>Red/Green</i> . Trinity River, Sheridan Bar .....	57
Figure 48.	Western Kootenai River Contour Plot, LUT Method .....	62

## LIST OF TABLES

Table 1.	Beer's Law $R^2$ Values, Kootenai River, Central Section.....	28
Table 2.	Beer's Law $R^2$ Values, Kootenai River, Eastern Section.....	32
Table 3.	Beer's Law $R^2$ Values, Kootenai River, Western Section .....	35
Table 4.	Beer's Law $R^2$ Values, Trinity River, Sheridan Bar .....	38
Table 5.	Beer's Law $R^2$ Values, Trinity River, Chapman Ranch.....	39
Table 6.	LUT $R^2$ Values, Kootenai River, Central Section.....	41
Table 7.	LUT $R^2$ Values, Kootenai River, Eastern Section .....	45
Table 8.	LUT $R^2$ Values, Kootenai River, Western Section .....	47
Table 9.	LUT $R^2$ Values, Trinity River, Sheridan Bar.....	48
Table 10.	LUT $R^2$ Values, Trinity River, Chapman Ranch .....	50
Table 11.	Beer's Law $R^2$ Values, Kootenai River, Eastern Section.....	51
Table 12.	Beer's Law $R^2$ Values, Trinity River, Sheridan Bar .....	53
Table 13.	LUT $R^2$ Values, Kootenai River, Eastern Section .....	56
Table 14.	LUT $R^2$ Values, Trinity River, Sheridan Bar .....	57
Table 15.	Lookup Table for Kootenai River.....	59

THIS PAGE INTENTIONALLY LEFT BLANK

## LIST OF ACRONYMS AND ABBREVIATIONS

DN	Digital Number
ENVI	The Environment for Visualizing Imagery
EOW	Edge of Water
FAA	Federal Aviation Administration
FMV	Full-motion Video
LIDAR	Light Detection and Ranging
LUT	Look-up Table
NIR	Near-Infrared
NRL	Naval Research Laboratory
<i>PWD</i>	Predicted Water Depth
ROI	Region of Interest
RTK	Real-time Kinematic
SOP	Standard Operating Procedure
TOA	Top-of-Atmosphere
UAV	Unmanned Aerial Vehicle
USGS	United States Geological Survey
WV-2	WorldView-2

THIS PAGE INTENTIONALLY LEFT BLANK

## **ACKNOWLEDGMENTS**

I would like to thank my advisors, Dr. Philip Durkee and Dr. Todd Holland, for their advice, assistance, guidance, and patience. Dr. Holland kept me focused when I started to stray or lose sight of the end, was the inspiration for one of the methods used here, and provided much of the data. I owe my interest in the subject to Dr. Durkee, as well as most of my understanding of the processes involved within this thesis. I also would like to extend a thanks to Kurt Nielsen for just listening to my ideas and answering many of my questions, no matter how trivial. A special thanks goes to Paul Kinzel at the U.S.G.S, who provided some of the data used, without which my thesis would never have gotten off the ground. Finally, my wife, Jennifer, deserves more thanks than I could put into words for being there when I was the most stressed, and for her understanding and support throughout my time here at Naval Postgraduate School.

THIS PAGE INTENTIONALLY LEFT BLANK

## I. INTRODUCTION

After the fall of the Soviet Union, Naval Operations shifted from a focus on blue water to a greater focus on littoral and fluvial environments. This has been driven by the acquisition of smaller vessels by nations requiring just coastal protection, as well as the emergence of pirate and terrorist activity in these coastal and inland waterways. To combat this, the U.S. Navy built Littoral Combat Ships for the near shore, as well as standing up Riverine Groups and Squadrons under Navy Expeditionary Combat Command. Unfortunately, Riverine Squadrons, as well as other U.S. forces that operate in these environments, are at a distinct disadvantage in not knowing the river terrain as well as the forces they are pursuing, especially when it comes to the ability to find navigable paths through the waterways. This has led to an enhanced need for analysis of river water depths, both on scene for a quick snapshot, as well as in-depth analysis at data production centers.

One method for acquiring this needed information is through the use of traditional hydrographic survey techniques. This would require the use of small boats with echo sounders to travel these waterways and collect data. Although highly accurate, this method is extremely time consuming and can be quite hazardous to the crew manning the vessel, and the vessel itself. Vessels would be placed in areas of unknown depth, with the potential of impassability. When considering the need for bathymetric data in hostile environments, personnel are potentially exposed to harm while their focus is on scientific data collection vice personal protection. Due to these issues, a different method needs to be considered, one utilizing remote sensing techniques.

Derivation of water depths from imagery collected via remote sensing is not a new field. For over thirty years, scientists have derived bathymetric data from images collected via satellite and manned aircraft (Lyzena 1978, 1980). The techniques that have been established have proven to be fairly accurate when examining coastal environments (Densham 2005; Loomis 2009). Issues arise when trying to transfer the collection methods from a coastal location inland to a fluvial environment. Rivers tend to be narrow while the resolution on many satellite imagers tends to be coarse. This

combination would mean that only a few pixels would represent water depths, and those pixels would most likely be contaminated with river bank or foliage info. Along with this, it is possible that the polar orbiting satellites used to collect this data will only catch a small section of the area of interest, if it collects it at all. To alleviate this, manned aircraft, which can carry the same hyper and multi-spectral sensors as well as light detection and ranging (LIDAR) sensors, could be flown to collect this imagery data. Resolutions would be higher and entire river sections could be collected. Aircraft used would be of the scientific nature, not war planes; coordination would need to be done, for these platforms that are not always readily available and would not be able to operate in hostile environments. For operational environments, manned aircraft would not be a viable option, so a different platform would need to be chosen. A platform that is readily available and has the ability to collect imagery.

Unmanned Aerial Vehicles (UAV) might be the solution to this issue. Most units, both large and small, have access to these aircraft. Some are large, like the MQ-1 Predator, and others are small, such as the RQ-11B Raven. The larger aircraft are able to carry larger sensors, but it is not known if they would be able to carry the hyper and multi-spectral sensors used in satellites, either do to capacity or mission constraints. Smaller vehicles have extremely small payloads, but since they are owned by the small units, such as Riverine Squadrons, have the ability to be tasked to do missions required by the units themselves. These UAVs typically only carry cameras, either full motion video (FMV) or still image, but these images are collected at lower altitudes and are of higher resolution. Operators of these aircraft are trained as UAV pilots, so no new training would be required; images would be collected using standard operating procedures (SOPs) and then post processed. Personnel trained to operate in hostile environments would be collecting the data themselves, and the aircraft itself is unmanned, putting minimal personnel at risk in hostile environments.

Utilizing standard images, those using digital numbers (*DN*) to represent pixel intensity vice radiance values, which describe the amount of light reflected off of a surface at a given angle, to derive bathymetry has been attempted in the past with good results. Fonstad and Marcus (2005) utilized a simple equation relating pixel intensity to

depth gained from flow rate and river width. Using these relations, they were able to apply values calculated to the rest of the image to create a bathymetric map. Similarly, Carbonneau et al. (2005) used the same equation to relate pixel intensity to measured depths, again creating bathymetric maps from imagery. The research conducted in this thesis will expound upon previous research, using the same equation, but different color bands and ratios of color bands, to determine which yields better results. Along with this, a simpler method will be attempted that would create a table relating pixel intensity to depth that can be easily used in the field.

THIS PAGE INTENTIONALLY LEFT BLANK

## II. BACKGROUND

### A. RADIATIVE TRANSFER FUNDAMENTALS

#### 1. Electromagnetic Theory and Radiative Transfer

Radiometry is the field that studies the measurement of electromagnetic, or radiant, energy. This field forms the “cornerstone of radiative transfer studies in natural waters” (Mobley 1994, p. 3). The electromagnetic spectrum encompasses wavelengths from gamma rays to radio waves. Near the center of this spectrum are the wavelengths that are of concern for derivation of bathymetry from imagery, visible light.

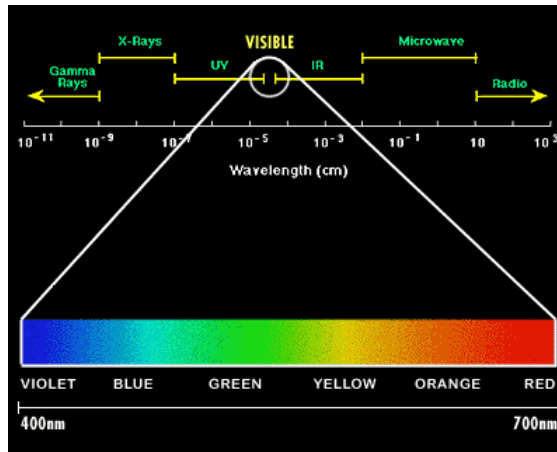


Figure 1. Visible light portion of electromagnetic spectrum (Image available from ScienceBuddies.org 2011)

In order to understand how bathymetry can be derived from images, a basic understanding of radiative transfer theory needs to be attained. The majority of light received at the Earth emanates from the sun (Mobley 1994, p. 6). Light reaches the Earth’s atmosphere where some photons, which are localized packets of electromagnetic energy, are scattered or absorbed by molecules in the atmosphere. Other photons pass through this medium, eventually reaching the Earth’s surface, and in this case the surface of the water. At this point, some photons are reflected off of the surface of the water while others pass through into this new medium. Within the water column, photons are again scattered and absorbed. Eventually, photons will reach the bed of the body of

water and be reflected back. Their journey reverses itself; photons are reflected, scattered, and absorbed, and finally reach the sensor.

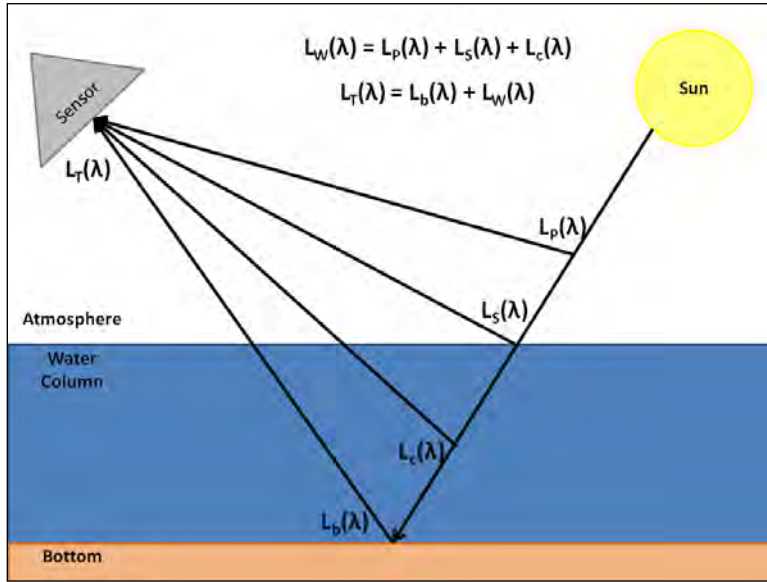


Figure 2. Radiative Transfer

The photons reaching the sensor are accounted for through four main sources (Legleiter et al. 2008):

$$L_T(\lambda) = L_b(\lambda) + L_c(\lambda) + L_s(\lambda) + L_p(\lambda), \quad (2.1)$$

where  $L_T(\lambda)$  is the total radiance reaching the sensor at a specific wavelength ( $\lambda$ ),  $L_p(\lambda)$  is the path radiance through the atmosphere,  $L_s(\lambda)$  is the surface reflected radiance off of the water,  $L_c(\lambda)$  is radiance from the water column, and  $L_b(\lambda)$  is the bottom reflected radiance, which is of primary interest for bathymetric mapping. In order to get to the bottom reflected radiance, the other sources contributing to the total radiance need to be accounted for, which can be difficult. All three, path, column, and surface reflected radiance, can vary from scene to scene. To account for these sources, Lyzenga (1981) suggests a method called deep-water correction, where radiance received over optically deep water (dark areas) is assumed to only have contributions from these three sources and is given by (Legleiter et al. 2008):

$$L_w(\lambda) = L_c(\lambda) + L_s(\lambda) + L_p(\lambda), \quad (2.2)$$

where  $L_W(\lambda)$  is the radiance observed over optically deep water. This value incorporates all inputs from the atmosphere into the total radiance received at the sensor. For long path lengths, such as from the Earth's surface to a satellite, these inputs cannot be ignored (Thomas and Stamnes, 1999, p. 35), and must be corrected for. It also incorporates inputs from the water column itself. For shallow, clear waters, this value can be considered small, and thus ignored. Substituting equation 2.2 into 2.1 gives:

$$L_T(\lambda) = L_b(\lambda) + L_W(\lambda), \quad (2.3)$$

Since measurements in ocean optics have shown that illumination is exponential with depth (Thomas et al. 1999, p. 362), this equation can then be represented empirically as given by Lyzenga (1978) and Philpot (1989):

$$L_T(\lambda) = L_b(\lambda) \exp[-c(\lambda)z] + L_W(\lambda), \quad (2.4)$$

where  $c$  is the extinction coefficient, which is a factor describing the change in intensity over the change in depth of the water, and  $z$  is the depth. In order to utilize this equation, a few assumptions need to be made. The first is that the optical properties of the water are homogenous in both the horizontal and vertical. Next, it is assumed  $L_W(\lambda)$  is constant throughout the scene, and finally, that a few values of  $L_T(\lambda)$  are known to allow for solving of  $L_b(\lambda)$  and  $c(\lambda)$ . Equation 2.4 and the assumptions made will be the basis for one method utilized for determining river depths.

## 2. Relating Radiance to Digital Numbers (DN)

Humans are visual creatures, depending on their eyes for 99% of the information received about their surroundings (Russ, 1995). When looking at the surrounding world, people do not see objects in a sense of radiance, but in a sense of color and brightness. Radiance, or spectral intensity, is a measure of the amount of light reflected or emitted from a point at a given angle, and is given in units of Watts per steradian per square meter ( $\text{Wsr}^{-1}\text{m}^{-2}$ ). This spectral intensity is analogous to the brightness, which is how the human eye differentiates between two objects of varying illumination in a scene (Thomas and Stamnes 1999, p. 45).

For remote sensing display purposes, radiance values are converted for each wavelength measured. The input received at the sensor, such as cameras, is seen as an intensity. The value at each pixel is converted to an electrical signal, sampled, and converted into a discrete integer (Schowengerdt 1997, p.22). This integer value, which typically ranges from 0 to 255 for display purposes, is called the digital number (*DN*). When seen on a display, the *DN* for a pixel in a specific scene is relative to the surrounding area for that specific scene. Since *DN* values range from 0-255, pixels in two separate images may have the same *DN* but in actuality may have different radiance values. The *DN* is relative to the specific scene for the given conditions, such as solar angle, illumination, atmospheric conditions, and sensor settings.

Typical equations for remote sensing deal with intensity in the form of radiance. The UAVs that will most likely be used to collect imagery are unable to carry massive sensors that are able to collect radiance values. Due to this, it is necessary to utilize these equations with data that can be collected, namely pixel brightness values in the form of *DN*. Since the sensors convert the radiance values into *DN* for display purposes, it is reasonable to assume, as Marcus and Fonstad (2005) had, that *DN* values can be substituted into equations where radiance is used, such as equation 2.4. For this assumption to be valid, the relation of radiance to *DN*, has to be linear, meaning that for every radiance value, only one *DN* can exist.

## **B. UAV ISSUES**

### **1. Imagery Collection**

One item to note has to do with the method in which the UAV camera, or imager, samples data. Traditionally, bathymetric derivations are done using satellites or other multi-spectral imagery collection platforms that measure the intensity of light and convert it to a *DN*. While a standard camera, or one used as the payload for a UAV, displays *Red*, *Green*, and *Blue* *DN* values, it is not in a true multi-spectral sense. The imager combines multiple wavelengths into each of the *Red*, *Green*, and *Blue* channels from the visible spectrum seen in Figure 1, which are then stored as *DN* for *Red*, *Green*, or *Blue*.

Although the values are not as exact for these three wavelengths as they would be for an multi-spectral imager, it will be assumed that they are relatively close.

## **2. Flight Issues**

The basis of this research was to utilize imagery collected from UAVs similar to those used operationally in the field. Due to Federal Aviation Administration (FAA) rules governing UAVs, it is not as easy as just launching an unmanned aircraft over the region of interest (ROI). Since airspace coordination is well outside the scope of this thesis, locations that were already approved for UAV use, contained suitable rivers for study, and had pre-existing UAV flights scheduled, were sought. Two such locations were found, one being Camp Roberts in California, and the other Fort Knox in Kentucky. Unfortunately, due to scheduling and timing issues, neither site was available for the timeframe needed, so proxy data was found to simulate imagery collected by a UAV.

## **C. TEST SITES**

In order for proxy data to be used, it needed to closely resemble imagery that could be collected by a UAV. With the always changing dynamics of rivers, the imagery used needed to have ground-truth bathymetry collected within a fairly reasonable window of time. For this research, two different types proxy data were found that met this criteria.

### **1. Kootenai River, Bonners Ferry, Idaho**

One of the larger tributaries of the Columbia River, the Kootenai River extends approximately 480 miles from its origin in British Columbia, Canada. It flows south through the Rocky, Purcell, and Salish Mountains into Montana and Idaho. It then turns back north where it empties into Kootenai Lake in British Columbia, Canada (*Wikipedia*, 2011). For this research, the region of interest is located near Bonner's Ferry, Idaho, with study areas being divided up by the USGS by geographic location: the meander reach, the braided reach, and the canyon reach. The focus here will be on the braided reach.

The braided reach portion of this section of the Kootenai River was chosen for a few different reasons. First and foremost was that the ground-truth data in this area was

more abundant and readily available when compared to the other two sections. Along with this, the braided reach had three distinct sections that could be examined. The eastern most section is the deepest of the three, the central section the straightest, and the western most section highly braided with what appeared to be the shallowest waters. Bottom type throughout the braided reach is predominately gravel with some cobble, alluvial sand, and bedrock outcroppings. These are most apparent in the shallower sections located in the west.



Figure 3. Kootenai River, Braided Reach



Figure 4. Eastern Section of Braided Reach



Figure 5. Central Section of Braided Reach



Figure 6. Western Section of Braided Reach

The imagery used for the Kootenai River was collected via WorldView-2 (WV-2) satellite, with a spatial resolution of 2 m. The imagery received was uncorrected and data associated with each pixel were radiance values. In order to simulate UAV imagery, data was corrected and converted to GeoTIFF format, whose process will be explained in Chapter III.

## 2. Trinity River, Junction City, California

Stretching approximately 165 miles, the Trinity River, located in Northern California, is the largest tributary of the Klamath River. The Trinity River begins in the

Scott Mountains in the Shasta National Forest. From here, it flows south into Trinity Lake, created by Trinity Dam, and then into Lewiston Lake, created by Lewiston Dam. Turning west-northwest, it flows along the southern side of the Trinity Mountains, receiving inputs from smaller rivers along the way. Eventually it meets with the Klamath River in Humboldt County (*Wikipedia* 2011).

For this research, the focus will be on sections of the river south of Junction City, California. Images were received from USGS in the Sheridan Bar and Chapman Ranch portions of the river. Each portion included multiple images, but two were selected initially for use for reasons similar to those for Kootenai River. In these images, ground-truth data was more abundant, providing better coverage of the river. In the Sheridan Bar image, fewer ripples were seen, meaning less sun glint and larger portions of the river available for study. Within the Chapman Ranch image selected, the deepest depths were observed, as well as fewer instances of ripples and sun glint. Bottom type, gravel, is fairly homogenous throughout all images, so it did not play a part in image selection.



Figure 7. Trinity River, Sheridan Bar, Image 271143



Figure 8. Trinity River, Chapman Ranch, Image 273138

Imagery provided by USGS was collected in April of 2009 via aircraft with a spatial resolution of 0.5 ft. The sensor type used is unknown, nor are the flight levels or collection times. The imagery was provided in GeoTIFF format, similar to what would be acquired via UAV, so no conversions were needed.

### **3. Ground-Truth (Bathymetry Data)**

Ground-truth data for both rivers was collected via LIDAR by the USGS. The data provided was referenced to ellipsoidal height and needed to be converted to a depth in order to correlate it to depths derived from imagery. Water levels on a river change regularly so the height of the edge of the water at the time of the image collection needs to be known. Rivers can also have slopes to them, where the height of the edge of the water in one location could possibly be higher, or lower, than a location further downstream. This change in height may not be linear as well, making changing heights to depths somewhat difficult.

For the Kootenai River bathymetry, height to depth conversion was done the Naval Research Laboratory, Stennis Space Center (NRL-Stennis), and then provided for ground-truth data. For the Trinity river, the USGS provided a file containing the ellipsoidal heights of the edge of water (EOW), which were collected with Real-Time Kinematic (RTK) GPS, that corresponded to the imagery. These values were taken and plotted in Matlab to reveal the slope of the line, which was not linear. Since EOW values

did not exist for every line of longitude of LIDAR data, a polynomial fit was done to fill in the gaps. Heights for these locations were then created, and then subtracted from the height of the river bed to give a depth at each bathymetric data point. This was done for all bathymetry covering the research area, and not just for the images that are being examined here.

## D. METHODS

Two different methods were chosen to test the feasibility of utilizing UAV imagery to derive river depths. One method utilizes radiative transfer theory and equations while the other simply relates a pixel intensity to a depth via a polynomial regression. Each method requires different inputs taken from in-situ measurements of the river. Accuracy of each method will be determined for the study areas when compared to ground-truth data.

### 1. Beer-Lambert-Bouguer Law

#### a. *The Equation*

The first method utilizes radiative transfer theory and expounds upon Equation 2.4. Beer-Lambert-Bouguer Law, or Beer's Law, describes the exponential absorption of light in water where scattering is minimal (Fonstad and Marcus, 2005). The equation is given here:

$$I(\lambda) = I_0(\lambda) \exp[-c(\lambda)z], \quad (2.5)$$

where  $I(\lambda)$  is the intensity of light at some depth at wavelength  $(\lambda)$ ,  $I_0(\lambda)$  is the intensity immediately prior to entering the water,  $c(\lambda)$  is the coefficient of extinction for that wavelength, and  $z$  is water depth. This equation is in the form where radiance values, typically *Red*, *Green*, and *Blue*, are used. It was shown earlier that  $DN$  can be substituted for  $I(\lambda)$ , which gives:

$$DN(\lambda) = DN_0(\lambda) \exp[-c(\lambda)z], \quad (2.6)$$

where  $DN(\lambda)$  is the pixel value at some depth and  $DN_0(\lambda)$  is the pixel value at a point just prior to entering the water. This value,  $DN_0(\lambda)$ , is called the value at zero depth, or the

point where the river makes contact with the river bank. As pointed out by Marcus and Fonstad (2005), this point needs to be one where the bank is wet, to represent the same wet reflective properties that the wet riverbed of the same composition would represent, as well as being shallow enough so the light cannot be acted upon by the absorbing properties of the water. The zero depth value can be acquired via in-situ measurements, where a person would mark the edge of the wetted riverbed via GPS, then use that point in the geo-rectified imagery, or by just examining the imagery and determining where the edge of the river is located.

This method requires one more in-situ measurement in order to work. To calculate the coefficient of extinction,  $c(\lambda)$ , a known depth with location has to be acquired and then matched to a pixel in the imagery. The equation is given as:

$$c(\lambda) = -\frac{\ln\left[\frac{DN(\lambda)}{DN_0(\lambda)}\right]}{z}, \quad (2.7)$$

This value can be calculated without a known depth, but it becomes an iterative process and requires other information, such as flow rate through a known river width (Marcus and Fonstad, 2005). Assuming that the river is well mixed both vertically and horizontally, and considered homogenous,  $c(\lambda)$  can be considered constant for the entire scene since it is an inherent optical property and depends only on medium (Mobley, 1994, p. 60). Knowing  $c(\lambda)$  then allows for depth values to be found at any pixel within a scene.

$$z = -\frac{\ln\left[\frac{DN(\lambda)}{DN_0(\lambda)}\right]}{c(\lambda)}, \quad (2.8)$$

Values at these single points can be calculated, or means of pixel values can be taken around a point, and then average depth can be calculated for a bin.

In simplest terms, Equation 2.8 gives the exponential relation between intensity, or the  $DN$  value of a specific wavelength or color band, and depth. As  $DN(\lambda)$  approaches  $DN_0(\lambda)$ , the natural log in the numerator approaches zero, and thus the depth approaches zero. As  $DN(\lambda)$  decreases exponentially, the numerator decreases and depths increase. This can be seen when examining Figures 4–8. As one gets closer to the banks

of the river, the color of the water brightens, and should mean shallower water; darker water color would then signify deeper water. This is dependent on the bottom type of the river. For the images here, the bottom type is predominantly gravel, so the bright, dry river banks mean that the shallower water would appear bright. If the bottom type were of a darker material, such as a dark rock covered in lichen, the exponential relation of water color to depth would still hold true, but would not be as apparent to the naked eye.

***b. Band Selection***

When using UAV imagery, three color bands are available for use: *Red*, *Green*, and *Blue*. In coastal and deep water application using multi and hyper-spectral imagery to derive depths, researchers typically use *Green* and/or *Blue* wavelengths. These wavelengths are absorbed slower by water, can penetrate deeper, and thus provide deeper depths. In a shallow water environment, neither *Green* nor *Blue* are extinguished fast enough to provide any delta in values, so previous research in this area utilized the *Red* wavelength (Marcus and Fonstad, 2005; Carbonneau et al., 2005). Only using one wavelength does introduce some problems, as found by Carbonneau et al. (2005). A single band can be affected differently by substrates having different albedos (Stumpf et al., 2003). A reflection off of one bottom type may appear brighter, or darker, than a reflection off of a different bottom type at the same depth, giving false results, and introducing noise into the data (Carbonneau et al., 2005).

To account for the variations in bottom types, the technique of using a ratio of bands was introduced and used in coastal areas with good results (Lyzena, 1978; Philpot, 1989; Stumpf et al., 2003; Densham, 2005; Loomis, 2009). As stated before, different bands attenuate at different rates through a water column, so at a given depth, one band will be less than another. A ratio of these two bands will also vary with depth. In theory, both bands should be affected similarly by a change in bottom albedo, or bottom type, and this change should be minimal when compared to the change due to attenuation with depth. Thus, the ratio of two bands over differing substrates at the same depth should remain constant (Stumpf et al., 2003).

Selecting two different bands, Equation 2.6 becomes:

$$\frac{DN(\lambda_1)}{DN(\lambda_2)} = \frac{DN_0(\lambda_1)}{DN_0(\lambda_2)} \exp\left[-\frac{c(\lambda_1)}{c(\lambda_2)} z\right], \quad (2.9)$$

and for simplicity, will be rewritten as:

$$DN(\lambda_{1,2}) = DN_0(\lambda_{1,2}) \exp[-c(\lambda_{1,2})z], \quad (2.10)$$

where  $\lambda_{1,2}$  represents the value of the ratio of two color bands for the given variable. As in equation 2.8, solving for depth gives:

$$z = -\frac{\ln\left[\frac{DN(\lambda_{1,2})}{DN_0(\lambda_{1,2})}\right]}{c(\lambda_{1,2})}, \quad (2.11)$$

For the ratio method to work, a ratio of two bands that attenuate differently in shallow waters need to be selected. Since *Green* and *Blue* both attenuate rather slowly in water, a ratio of the two is not a wise selection. In previous research, it was suggested that the bands used be separated by at least 10 nm (Fonstad and Marcus, 2005), meaning that a ratio *Red* and *Blue* should be used, or one of *Green* and *Near-Infrared (NIR)*. Since *NIR* is not typically available with UAVs, the focus will be on the use of a *Red/Blue* ratio, but single band values calculations, as well as a ratio of *Red/Green*, will still be computed for comparison.

## 2. Look-up Table (LUT) via Polynomial Regression

Other methods have been attempted previously relying on LUTs and regression, and not on radiative transfer equations. One such method uses hyper-spectral imagery and LUTs, but is extremely complicated. Multiple LUT databases are constructed for different variables and circumstances. Using these databases, water depth is calculated (Mobley et al. 2005). Although a good method, it is too complicated for use in the field. Another method uses a linear regression and all three color bands. Coefficients for each color band are tuned using multiple in-situ depth measurements. Once coefficients are known, the linear equation is applied to the entire scene to create predicted water depths (*PWD*) (Lejot et al. 2007). Once again, this an interesting method, but is too complicated for field use.

A simpler method, which does not utilize radiative transfer equations, will be attempted in this research. This method will utilize polynomial regression to approximate the exponential relation of water color to depth. To best represent the exponential curve, a third order polynomial equation will be used:

$$z = p_3[DN(\lambda)]^3 + p_2[DN(\lambda)]^2 + p_1[DN(\lambda)] + p_0, \quad (2.12)$$

where  $z$  is the depth of the water,  $DN(\lambda)$  is the value of the pixel, and  $p_{\#}$  is the coefficient for the respective order. For simplicity, lower order equations could be used, but would do poorly at representing the attenuation of light in water. A first order equation is linear, and would not see the exponential curve at all; second order would do a better job of approximating the curve, but would not show an inflection point if there was one. A third order polynomial will represent the exponential curve, and since a second derivative is needed to show inflection points, will also be able to approximate this. Higher order equations could be used, but don't gain much more in representing the exponential curve and add more complexity to a method that should be simple. Although technically similar to the Beer's Law approach, one possible advantage of this method over Equation 2.8 is that the third order polynomial could fit relations not strictly governed by the exponential relation between light and water that is assumed.

For this method to work properly, more in-situ measurements will be needed than in the Beer's Law method, which used only two pairs of depth to intensity. For a third order polynomial that has three unknowns, at least three in-situ measurements would be required; for a better representation, more in-situ points would be needed. Depths at varying locations need to be collected that correspond to different pixel values on an image. To provide the best representation via polynomial regression, measurements should be collected over varying depths, and enough to represent the exponential attenuation response of light in water. The amount of in-situ depths collected does not need to be extremely high, and should only be on the order of ten. With these values, the coefficients,  $p$ , can be calculated using the *polyfit* function in Matlab for each color band, or ratio of color bands, used. The *polyfit* function works by creating an equation of a line,

or curve, that best represents the data supplied. In this case, depths and their corresponding  $DN(\lambda)$  are given and the function creates coefficients that would best fit the curve.

With the coefficients calculated, depths can be found for pixel values within the range used to create the third order equation. The  $DN(\lambda)$  values would correspond to a point on the curve that is given by Equation 2.12, and this point on the curve would correspond to some depth. These values will then populate a LUT that should be easily correlated to individual pixel intensities on an image to depths.

All three color bands, and both ratios, will be used to test the LUT method. Using the same points collected for the Beer's Law method allows for less computing time, but more importantly, allows for the comparison of the two methods.

THIS PAGE INTENTIONALLY LEFT BLANK

### III. METHODOLOGY

#### A. IMAGE CORRECTION

##### 1. Kootenai River

Prior to any analysis being completed on the WV-2 imagery collected, it needed to be corrected for atmospheric inputs and converted to a format similar to what would be collected from a UAV. Since the values received by the satellite are unique to the calibration of the sensor, conversion to Top-of-Atmosphere (TOA) reflectance produces data that can be compared to other data with the same base line.

To accomplish this, the image was opened in ENVI (The Environment for Visualizing Images) and using steps outlined by DigitalGlobe (2005) and Green et al. (2000), mathematical corrections were applied to every pixel in the image. These steps included converting values to reflectance ( $\rho$ ) from radiance, and then removing inputs from atmospheric reflection. The method outlined by Lyzenga (1981) for removing these atmospheric inputs calls for utilizing optically deep water and assumes all inputs are from the atmosphere and water column. Unfortunately, there did not appear to be optically deep water in the scene, so another approach needed to be taken. Dark pixel subtraction, which is similar to the deep water approach, was done using deep shadow over a asphalt pavement. The assumption is that this surface has zero reflectance and all inputs are from the atmosphere (Green et al. 2000, p.115). With atmospheric inputs removed, water column inputs needed to be accounted for. It is then assumed that since the water is shallow, and relatively clear, these inputs are negligible, and that light emanating from the water is due to bottom reflectance.

With the image corrected to TOA reflectance, it was then converted to a GeoTIFF to represent imagery collected from a UAV. Utilizing ENVI, each band at every pixel was sampled at 8-bits, converting the reflectance value for *Red*, *Green*, and *Blue* to a value from 0-255. When the conversion is complete, each pixel has the same geo-location as the original image, but instead of a three reflectance values, it has three *DN* associated with it.

## **2. Trinity River**

Images received from the USGS of the Trinity River were in GeoTIFF format, similar to images that would be collected from a UAV, so no conversions needed to be done. Assumptions do need to be made to account for all the inputs that make up the total radiance as see in equation 2.4.

One main input to total radiance is energy due to atmospheric interactions. This energy needs to be accounted for when the path length through the atmosphere is long (Thomas and Stamnes 1999, p. 35). In this case, the height of the aircraft is not known, but it is assumed to be fairly low flying, at approximately 2000 m, creating a short path length through the atmosphere. Along with this, the elevation of Junction City, CA, about 2600 ft, should mean that the atmosphere is drier than if it were at sea level, but by no means as dry as if it were at higher elevations. Using these assumptions about atmospheric conditions at elevation and height of the aircraft, energy due to atmospheric conditions will be considered very small compared to bottom reflectance, and ignored (Legleiter et al., 2008).

Sea-surface reflections and water column interactions are two other inputs that need to be accounted for. Sea-surface reflections were considered to be negligible since areas with sun-glint were removed prior to any calculations being conducted. As for water column inputs, it is assumed that since the water is shallow, and relatively clear, these inputs are negligible, and that light emanating from the water is due to bottom reflectance.

## **B. REGION OF INTEREST (ROI) SELECTION**

### **1. Kootenai River**

As stated before, the image was divided in three sections that represented different river characteristics. Using ENVI, three ROIs were created by selecting wetted portions of the river from the imagery, and excluding areas that were shadowed, contained dry bank, or any type of over-hanging foliage. ROIs were selected by hand and not through any classification techniques, with each having a varying amount pixels: 48,000 in the eastern section, 71,000 in the central, and 186,000 in the western section.

Zero-depth location was chosen once main ROIs were selected. Looking at the image, the edge of the water can be easily discerned (see Figures 3–6). The bottom is predominately gravel, and when dry appears as a bright white on the image. The point where the gravel changes color was chosen as zero-depth, with 24 points selected and a mean taken to provide the input value ( $DN_0(\lambda)$ ) for Equations 2.7 and 2.11.

A fixed depth also needed to be selected in order to calculate the extinction coefficient for the image. For each ROI, this was done by choosing a depth from the ground-truth data. Then, using ENVI, the pixel that corresponded to this point was found, the mean of the surrounding area taken, and the associated DN for each band recorded.

## **2. Trinity River**

Two main images were selected to work with from within the Trinity River imagery. Using ENVI, ROIs were selected within each of these images. Regions were selected by hand and chosen to eliminate shadows from over-hanging shrubbery and sun-glint due to ripples caused by bottom interactions or wind. The regions that are depicted in the imagery are not large, but with the amount of data points available due to the small spatial resolution, ROIs range between 200,000 and 400,000 data points.

For each image, separate zero depth points needed to be selected for use in Equations 2.7 and 2.11. As was the case with Kootenai River, the bottom type here is predominately gravel, and when dry, is easily discernable from the wetted areas. This can be seen in Figures 7 and 8. Areas were chosen near the edge of the water, containing 98 points for the Sheridan Bar and 45 for Chapman Ranch, and an average was taken of each to be used as  $DN_0(\lambda)$ .

Fixed depths also needed to be found to calculate the extinction coefficients for each section. Using the RTK file that accompanied the ground-truth data, a known depth for each image was found and its location correlated to an average pixel value on the imagery. The values for each band were recorded, and then values for the ratios of *Red/Green* and *Red/Blue* were calculated.

## C. DEPTH DERIVATIONS

### 1. Beer's Law

#### a. Kootenai River

With the image corrected, and the ROIs selected, the data from ENVI was outputted to an ASCII text file containing coordinates and *Red*, *Green*, and *Blue* values for each pixel. This file was then read into Matlab where all processing would occur. Code was written to first calculate extinction coefficient for each band, and then for each ratio of bands. The extinction coefficient could then be used to calculate depths at given pixel locations.

Since the ground-truth data had so many fewer points, ten-thousand for the entire river vice tens of thousands for each section, the ground-truth locations were used to take samples from the ROI data. This also allows for easy comparison since the known value locations are being used to select pixels to calculate depths from. For each ground-truth point, pixel values within a certain radii, 1 m, 2.5 m, 5 m, or 7.5 m, were found. These radii were chosen based on the pixel size, 2 m, and the spacing between ground-truth points, 15 m. To account for any sun glint off of ripples due to wind or bottom interaction, the mode of the sample was found along with a standard deviation. Any *DN* found to be higher than the mode plus the standard deviation and error allowance of two *DN* were removed from the data. The mean of the remaining sample was then found and stored for use in Equation 2.8 as a single band calculation. When ground-truth point had associated mean pixel values for all three bands, *Red/Blue* and *Red/Green* ratios were found for each point and stored for use in equation 2.11.

*PWD* were then calculated for each ground-truth point. To test the accuracy of the calculations, the coefficient of determination ( $R^2$ ) was used. Previous research by Carbonneau et al. (2006) and Fonstad and Marcus (2005) used this value as a measure of accuracy, so it was used here as well.

Calculation of water depths using Beer's Law was completed for each radii: 1 m, 2.5 m, 5 m, and 7.5 m, each band: *Red*, *Green*, *Blue*, *Red/Blue*, and *Red/Green*, and each location: central section, western section, and eastern section, producing 60 plots for comparison.

***b. Trinity River***

The ROI data created in ENVI was ingested into Matlab in the same manner as described for Kootenai river. The same Matlab code was used to process the data, so coefficients were first calculated and pixel values for each band were found for corresponding ground-truth depths at radii of 0.5 ft, 1 ft, 2.5 ft, and 5 ft. These radii were selected base on the spatial resolution of the imagery, and the width of the river, which is approximately 100 ft wide. With the pixel values found, the same quality control was performed to ensure that pixels contaminated by sun glint or other factors were removed, and then the mean pixel value for each band, at each ground-truth depth was found, with bin size determined by the search radius. These pixel values were then used to calculate the ratios of *Red/Green* and *Red/Blue* at the same points.

**2. LUT via Polynomial Regression**

***a. Kootenai River***

To begin creating the LUT, additional points were needed that represented varying depths through the river and correlated to different pixel *DN* values. Examining the ground-truth data, depths in the river varied from approximately 0.5 m to in excess of 11 m. Points were chosen based on variations in depth of 0.5 m, starting at 1.5 m. At 6 m depth, values for *Red* remained near constant, staying at or about  $DN = 5$ . Due to this, any actual depth deeper than 6 m would appear to be at 6 m, so this is the maximum depth chosen for the polynomial regression. A total of 10 points were used for the polynomial regression in the Kootenai River.

Using the *polyfit* function in Matlab, coefficients for a third order equation were created for each band and the ratios of *Red/Green* and *Red/Blue*. With these coefficients, pixel values that were collected in the Beer's Law method were applied to

equation 2.12, and depths found. With the amount of points used, it was simpler, and faster, to insert pixel values directly into equation 2.12 than to search for the values in a table, but the results would be the same. Using the same points and values used Beer's Law method for Kootenai River produces the same amount of plots and allows for comparison between the two methods.

***b. Trinity River***

For LUT creation, additional points were collected that represented varying depths for varying pixel values. At Sheridan Bar, depth selection started at 2 ft and went to 5 ft, at 0.5 ft increments, giving a total of 7 points. Very few ground-truth points existed shallower than 2 ft or deeper than 5 ft, and for those that did exist, very little variation in  $DN$  occurred. For Chapman Ranch, depth selection began at 1.5 ft and went to 5.5 ft, giving 9 points for the polynomial regression. Depths were observed in excess of 10 ft, but few ground-truth points were available in the area. Abundant ground-truth points existed up to 7 ft, but beyond 5.5 ft, little variation in  $DN$  occurred, so these depths were left out of the polynomial regression.

With the values for the Trinity River collected, the same methods as described for Kootenai River were applied to create the LUT here. The *polyfit* function in Matlab was used to create coefficients for equation 2.12. Pixel values collected in the Beer's Law method were then applied to the equation to determine depths, and since the same points were used for both methods, comparisons between the two could be done.

## IV. RESULTS

Prior to examining the actual depth derivations, it is important to take a look at the relation of pixel intensity to depth. It was assumed that with depth, pixel intensity for color bands would attenuate exponentially, especially for *Red*. As an example, Figure 9 shows the relation of *DN* for the color band *Red* to actual depth for the central section of the Kootenai River, where an exponential decay can be seen for the plot of the *DN* values. The exponential curve plotted using Beer's Law, seen in red, follows nicely at deeper depths, but strays in water shallower than 2 m. The equation created using Beer's Law would need to be adjusted in order to fit the actual exponential attenuation. The LUT method, plotted in green, mimics the exponential curve in deeper water, but tracks much better in shallower waters. This graph shows that although light attenuates exponentially with depth, this assumption is only an approximation as can be seen by the plot of LUT via polynomial regression when compared to the actual exponential curve.

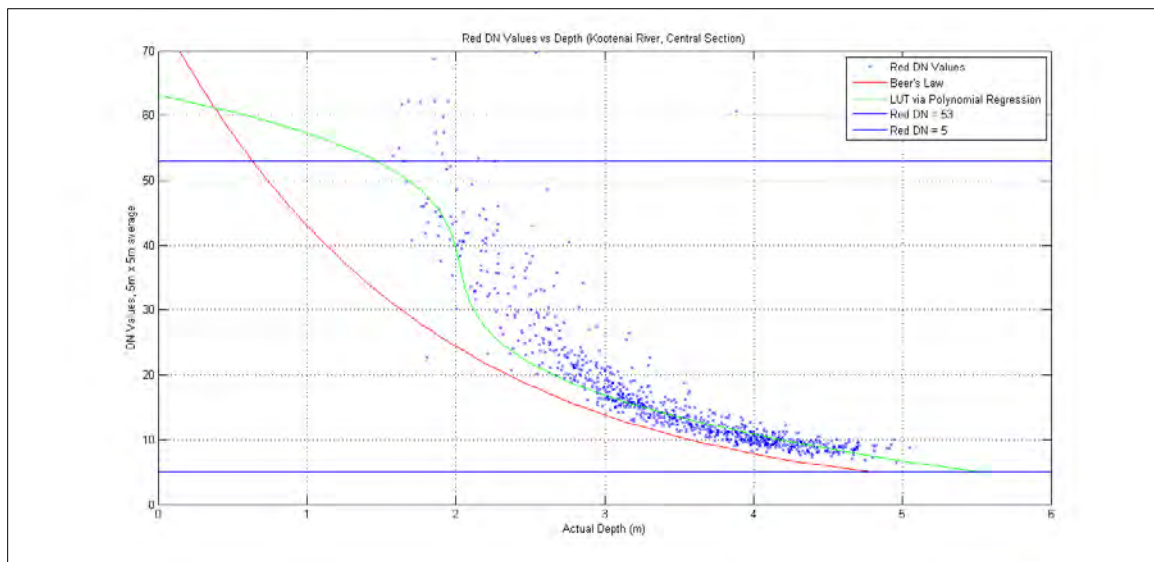


Figure 9. *Red DN* values versus depth for Kootenai River, Central Section. Red line represents exponential curve for Beer's Law and Green line represents curve plotted using LUT via polynomial regression. Blue lines represent the bounds used to create polynomial coefficients for LUT.

## A. BEER'S LAW

### 1. Kootenai River

#### a. Central Section

Table 1 shows the  $R^2$  values for the  $PWD$  compared to the actual water depth, where  $D$  represents the radius around the ground-truth points and  $N$  is the amount of ground-truth points that were used. Some ground-truth points lie just outside the ROI created in ENVI, so at smaller radii, these ground-truth points do not have pixels associated with them and are neglected. As the radii increases, pixels come within range, and more ground-truth points can be used. Except for *Red/Blue*, all the bands did best with a radius of 7.5 m, or 15 m diameter. Although 7.5 m radius had the highest  $R^2$  values, and covered the distance between ground-truth points, which were separated by 15 m, it produces a large area to calculate a single depth. For this reason, it doesn't seem reasonable to use such a large area to derive depths, especially when  $R^2$  values for radii of 2.5 m and 5 m are fairly close. For the central section, 2.5 m values, where *Red/Blue* had the highest  $R^2$  values, will be used to compare the three different bands.

Table 1. Beer's Law  $R^2$  Values, Kootenai River, Central Section

	D = 1 m N = 837	D = 2.5 m N = 868	D = 5 m N = 921	D = 7.5 m N = 961
Red	0.865	0.886	0.893	0.896
Green	0.817	0.843	0.853	0.861
Blue	0.614	0.680	0.728	0.751
Red/Green	0.810	0.861	0.878	0.879
Red/Blue	0.871	0.912	0.910	0.903

*Blue*, which showed the least amount of variation in  $DN$  with depth, did the worst, with  $R^2$  varying from 0.614 at 1m radius to 0.751 for 15m radius. When examining the plot for *Blue* at 2.5 m (Figure 10), depths shallower than 2.5 m to 3 m did not correlate well. Correlation at depths beyond this were better, and the depths calculated are close to the actual measured depths.

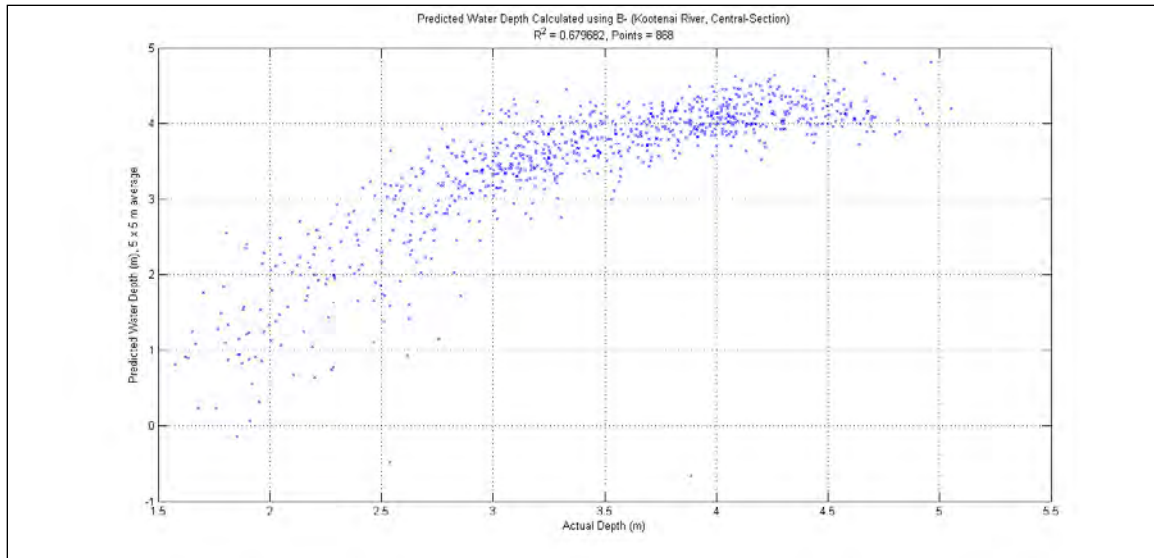


Figure 10. *PWD* Calculated using *Blue*. Beer's Law, Kootenai River, Central Section

Calculations for both *Green* and *Red/Green* correlated well and had  $R^2$  values fairly close to one another. Like *Blue*, *Green* did not correlate depths well at depths shallower than 2.5 m, but correlated much better at deeper depths as well as calculating values fairly close to actual depths, as can be seen in Figure 11. Examining Figure 12, *Red/Green* did a better job of calculating depths in shallow water, but under-predicted all depth values by about 1 m.

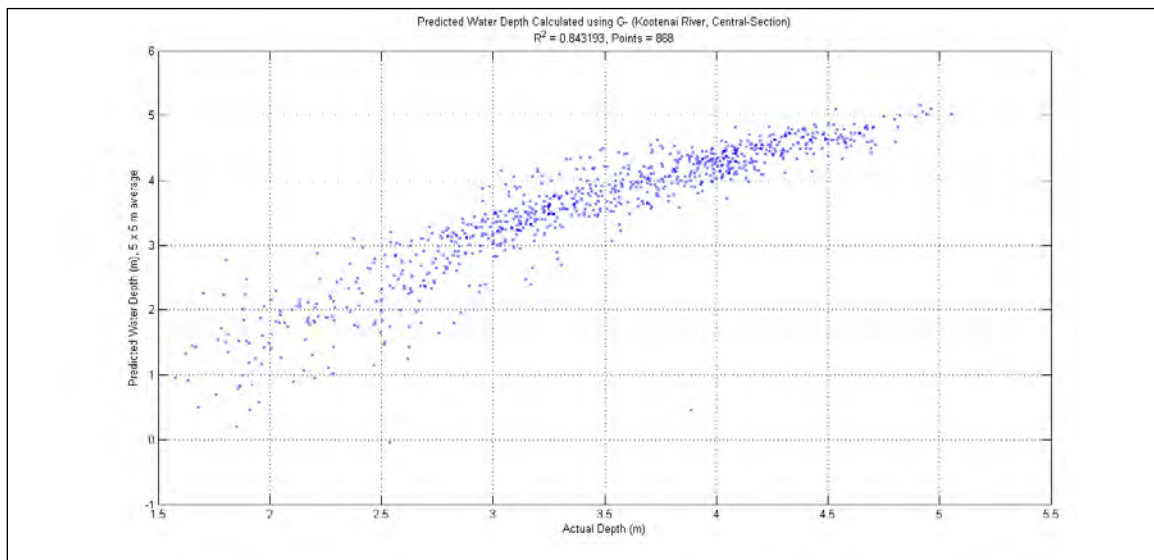


Figure 11. *PWD* Calculated using *Green*. Beer's Law, Kootenai River, Central Section

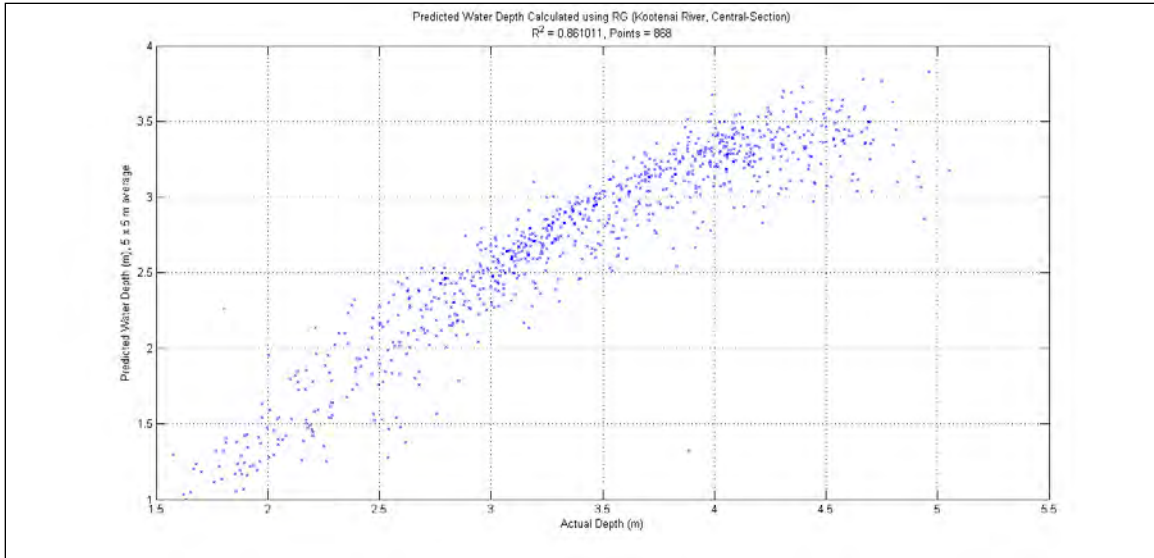


Figure 12. *PWD* Calculated using *Red/Green*. Beer's Law, Kootenai River, Central Section

In previous research (Fonstad and Marcus, 2005; Carbonneau et al., 2006), *Red* was used as the band to calculate water depths with Beer's Law. Used again here, *Red* did well, with  $R^2 = 0.886$ . In shallower depths, values are not grouped as close together as in deeper waters, as shown in Figure 13. Depth values are also under predicted by about 1 m in shallow and 0.5 m in deeper water.

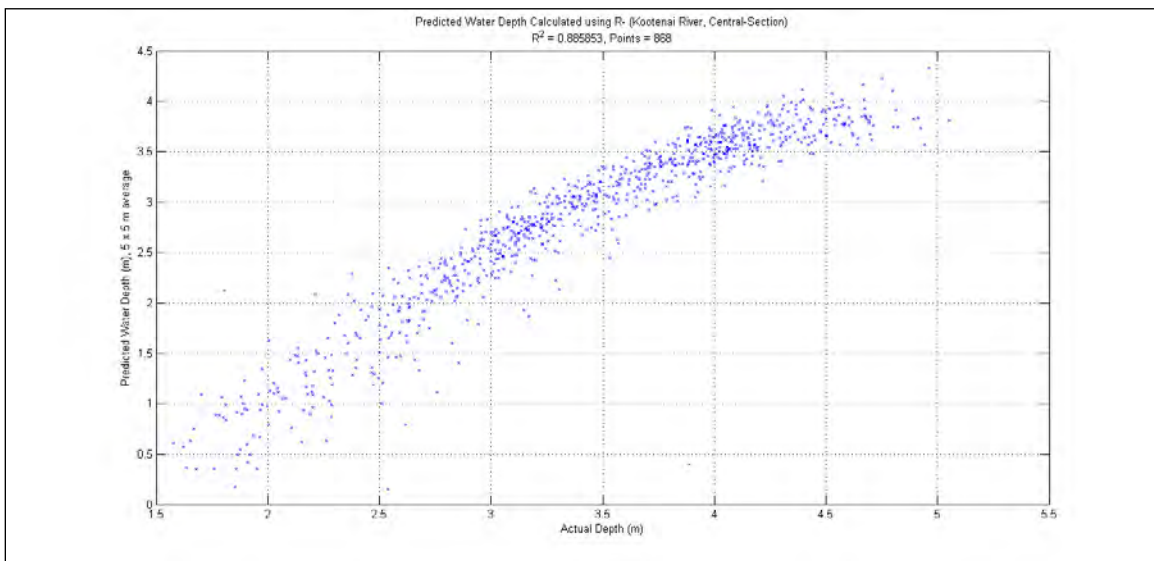


Figure 13. *PWD* Calculated using *Red*. Beer's Law, Kootenai River, Central Section

Figure 14 shows *PWD* for *Red/Blue*, which had an  $R^2$  of 0.912 at 2.5 m radius, which was the highest coefficient of determination for all radii and bands. Examining the plot, the grouping in shallow water is better than that for *Red* and continues through to deep water. Depths are still under predicted, but the offset appears to be almost a constant 1 m.

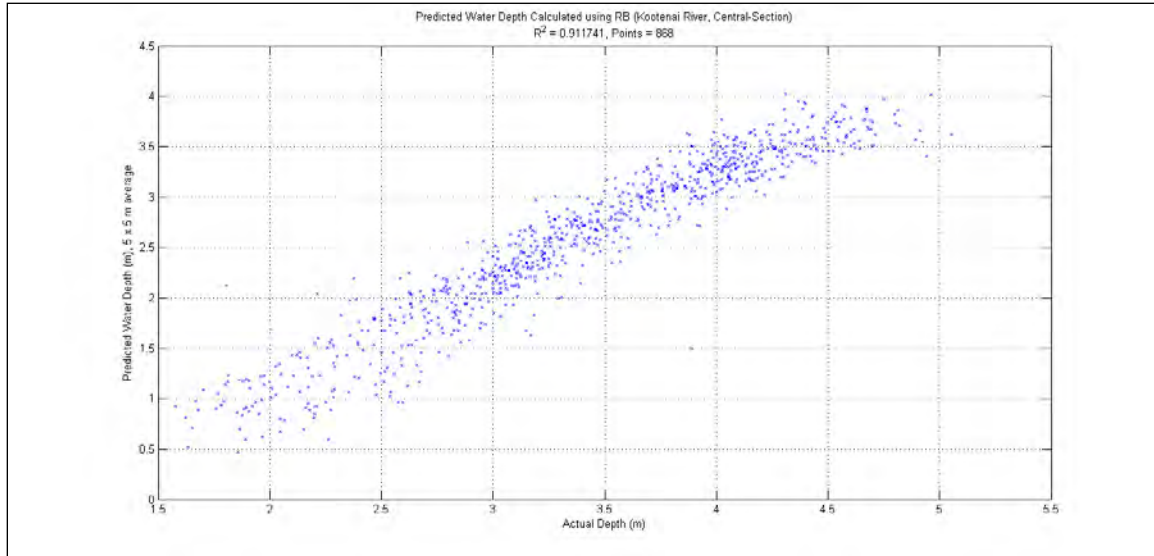


Figure 14. *PWD* Calculated using *Red/Blue*. Beer’s Law, Kootenai River, Central Section

***b. Eastern Section***

Table 2 shows  $R^2$  values for *PWD* using Beer’s Law in the Eastern Section of the Kootenai River, which had the fewest ground-truth points and deepest depths. A radius of 7.5 m has the highest correlation between *PWD* and actual depths, but for the same reasons described in the Central Section, a radius of 2.5 m would be a better representation of pixel values around a single depth, and will be used when comparing the different bands.

Table 2. Beer's Law  $R^2$  Values, Kootenai River, Eastern Section

	D = 1 m N = 562	D = 2.5 m N = 598	D = 5 m N = 638	D = 7.5 m N = 674
Red	0.427	0.434	0.442	0.469
Green	0.509	0.519	0.535	0.559
Blue	0.285	0.311	0.322	0.344
Red/Green	0.184	0.224	0.249	0.282
Red/Blue	0.417	0.439	0.445	0.477

In this section of the river, all  $R^2$  values are much lower than those in the Central Section. *Green* had the highest correlation at 0.519 for a radius of 2.5 m. The values of *Red* and *Red/Blue* were fairly close in  $R^2$ , with *Red/Blue* having a slightly higher value. Calculations using *Red/Green* and *Blue* did the worst in this section. When examining the plots for the different bands, Figures 15–19, one reason for the lower correlation is due to the maximum depth that is able to be calculated. When gathering depths and corresponding  $DN$  for the LUT, it was found that beyond 6 m, where the bottom can no longer clearly be seen,  $DN$  values for each band remained almost constant, and anything deeper than 6 m would most likely appear as 6 m. As can be seen in Figures 14–18, this is the case for all bands, as well as all depths being under-predicted.

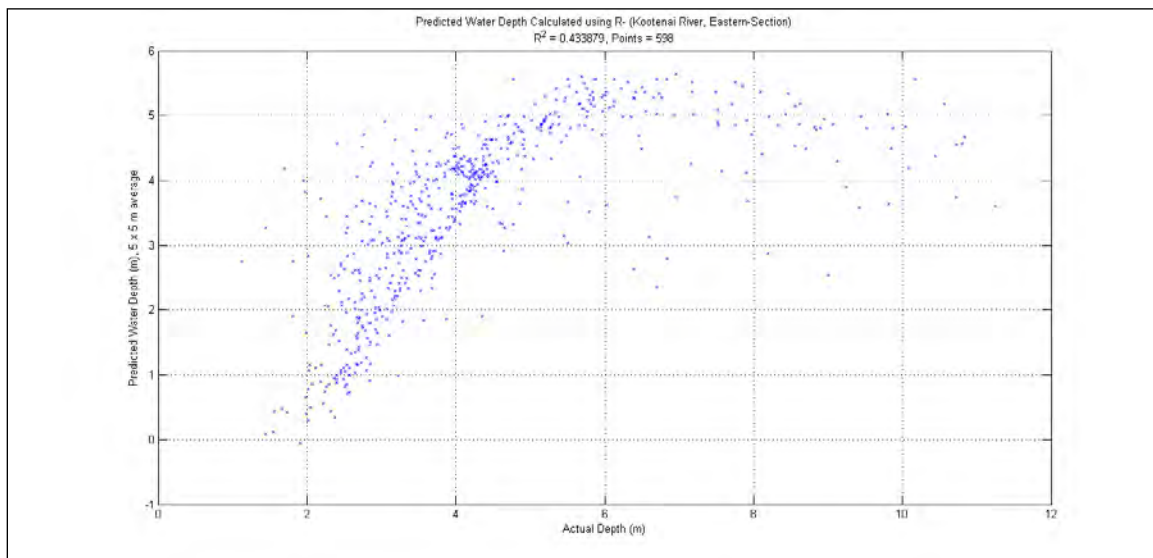


Figure 15.  $PWD$  Calculated using *Red*. Beer's Law, Kootenai River, Eastern Section

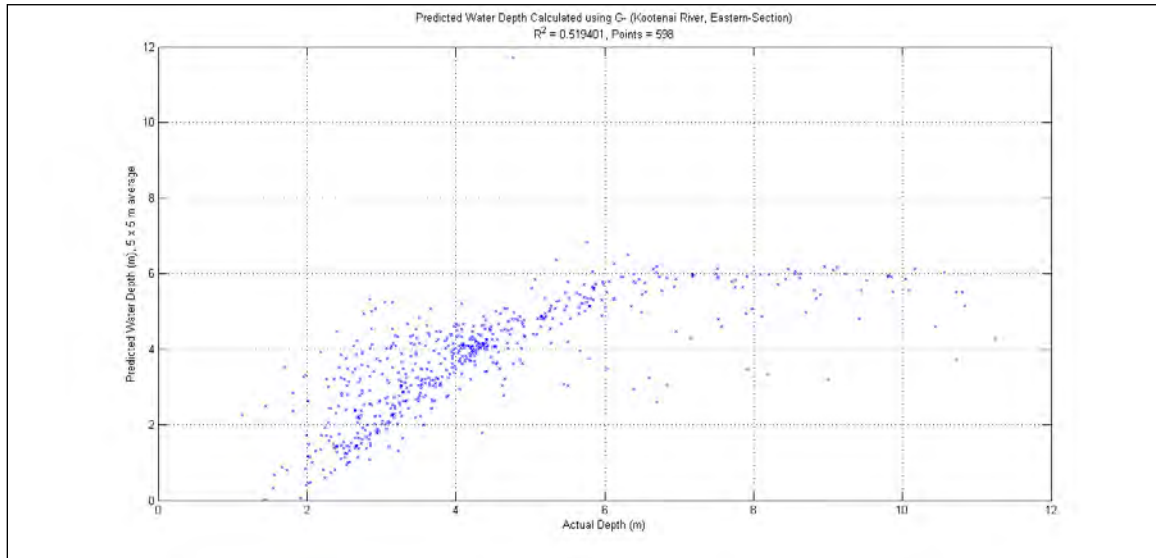


Figure 16. *PWD* Calculated using *Green*. Beer's Law, Kootenai River, Eastern Section

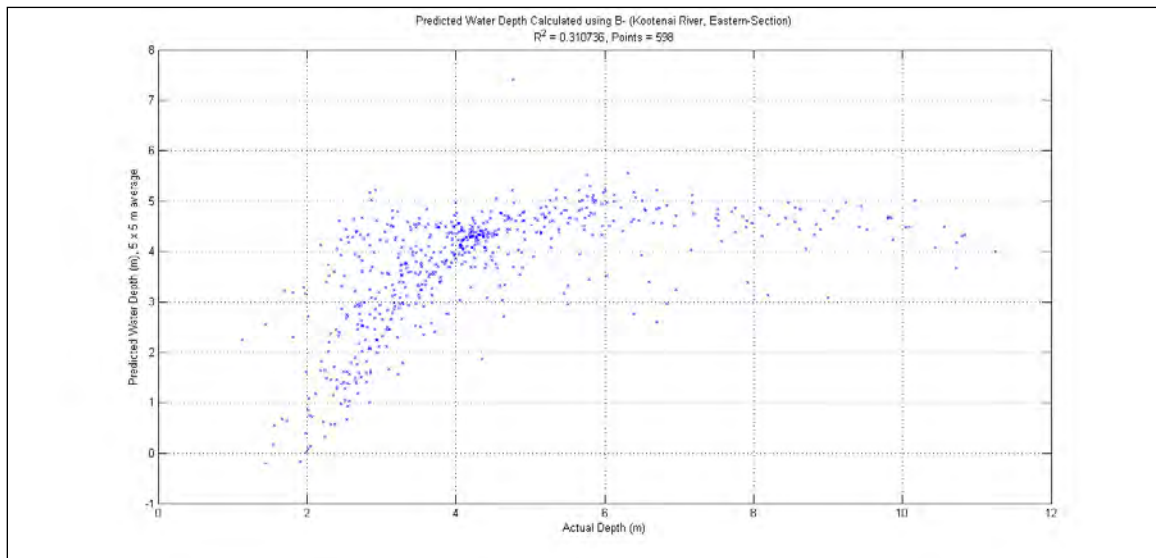


Figure 17. *PWD* Calculated using *Blue*. Beer's Law, Kootenai River, Eastern Section

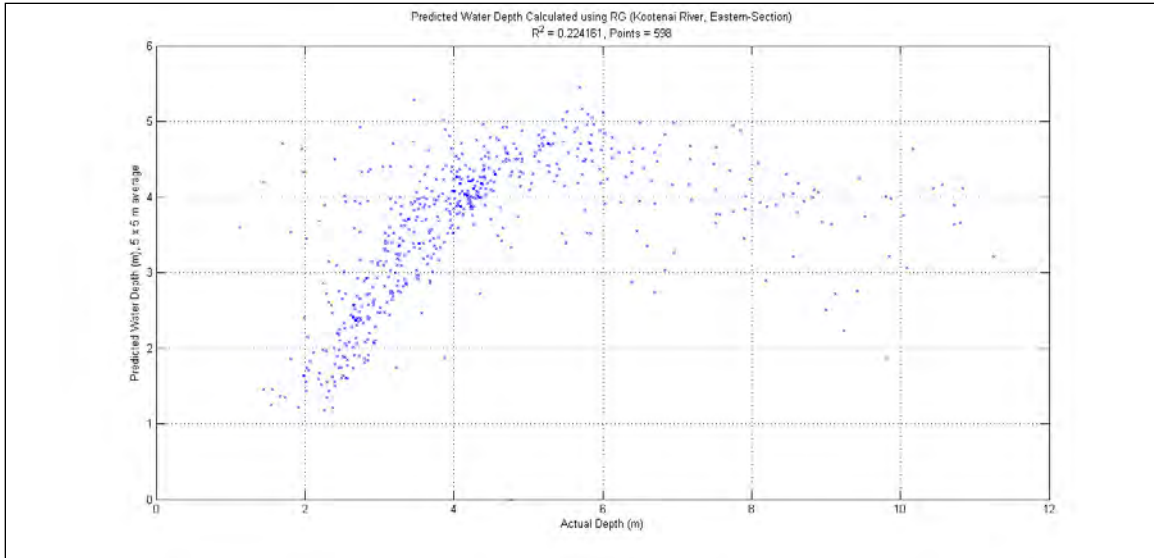


Figure 18. *PWD* Calculated using *Red/Green*. Beer's Law, Kootenai River, Eastern Section

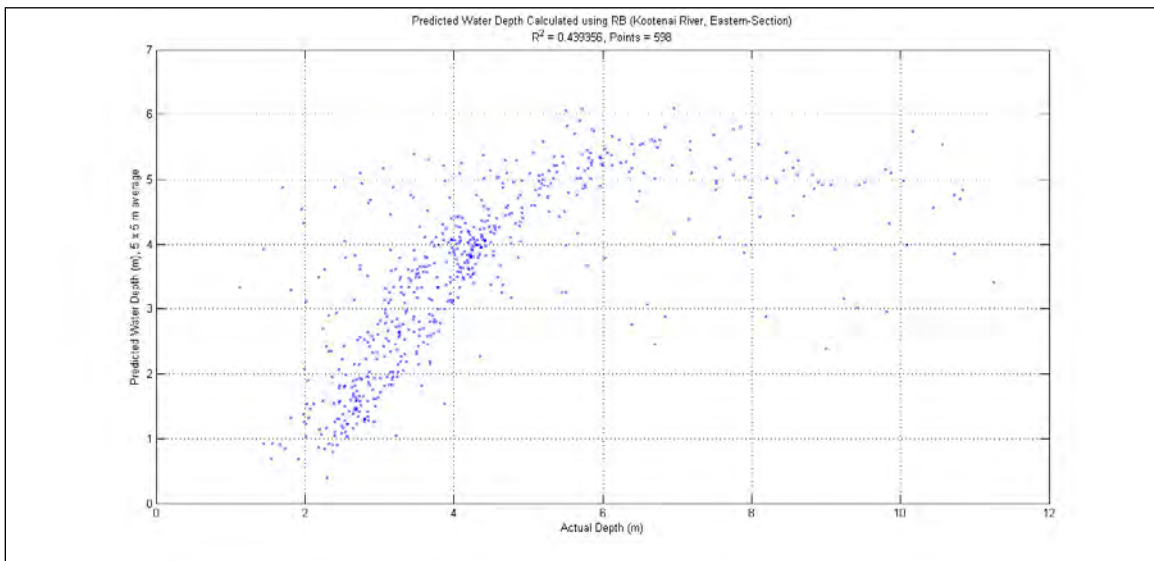


Figure 19. *PWD* Calculated using *Red/Blue*. Beer's Law, Kootenai River, Eastern Section

**c. Western Section**

Table 3 shows  $R^2$  values for *PWD* using Beer's Law in the Western Section of the Kootenai River, which was the largest of the three sections. Unlike the other two sections, a smaller radius of 5 m showed the highest correlation values. To

keep consistent with the other two sections, a radius of 2.5 m was used, which also contains the highest correlation value for *Red/Blue*.

Table 3. Beer's Law  $R^2$  Values, Kootenai River, Western Section

	D = 1 m N = 2194	D = 2.5 m N = 2291	D = 5 m N = 2435	D = 7.5 m N = 2606
Red	0.675	0.672	0.681	0.661
Green	0.516	0.524	0.555	0.551
Blue	0.336	0.342	0.367	0.372
Red/Green	0.653	0.663	0.662	0.635
Red/Blue	0.742	0.750	0.748	0.717

For this section of the river, all bands suffered from an under prediction of water depths, as was the case before. Using *Blue* by itself did the worst, and *Green* fared only slightly better. *Red* has a fairly high correlation, but when looking at Figure 20, *Red* actually predicts negative, or above the surface of the water, depths. This is also the case for *Green* and *Blue*. The ratios of *Red/Green* and *Red/Blue* both do very well, with neither predicting negative depths, and *Red/Blue* having the highest correlation of 0.750. For both cases, depths greater than 6 m do not correlate well to actual depths.

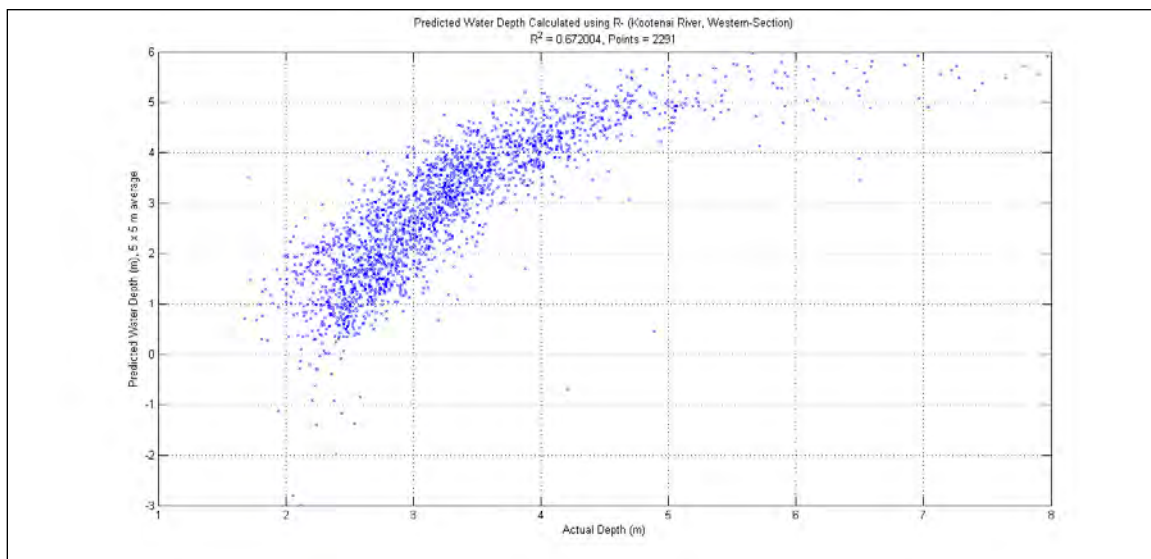


Figure 20. *PWD* Calculated using *Red*. Beer's Law, Kootenai River, Western Section

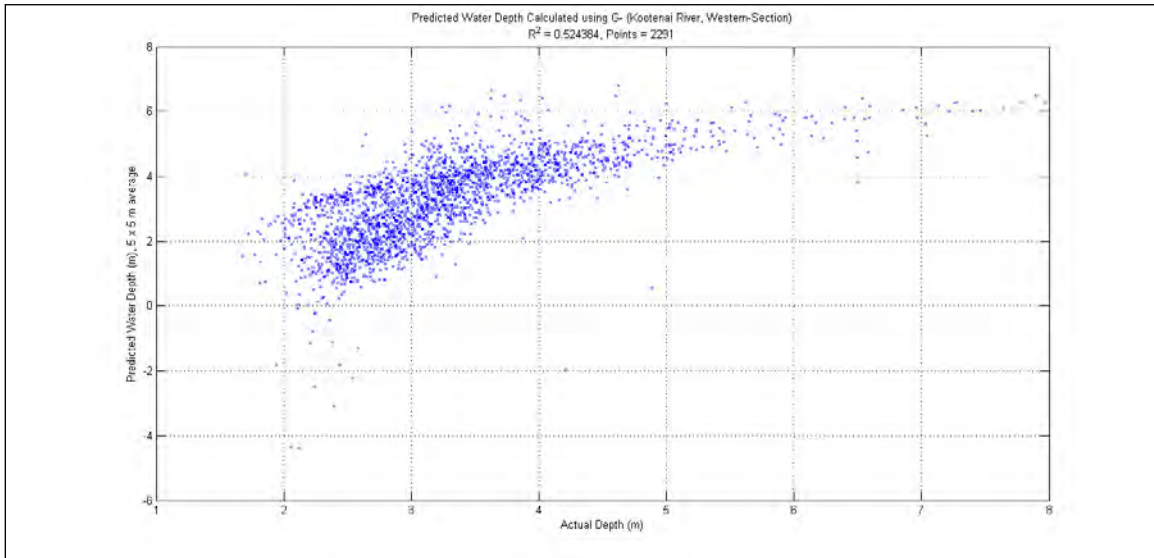


Figure 21. *PWD* Calculated using *Green*. Beer's Law, Kootenai River, Western Section

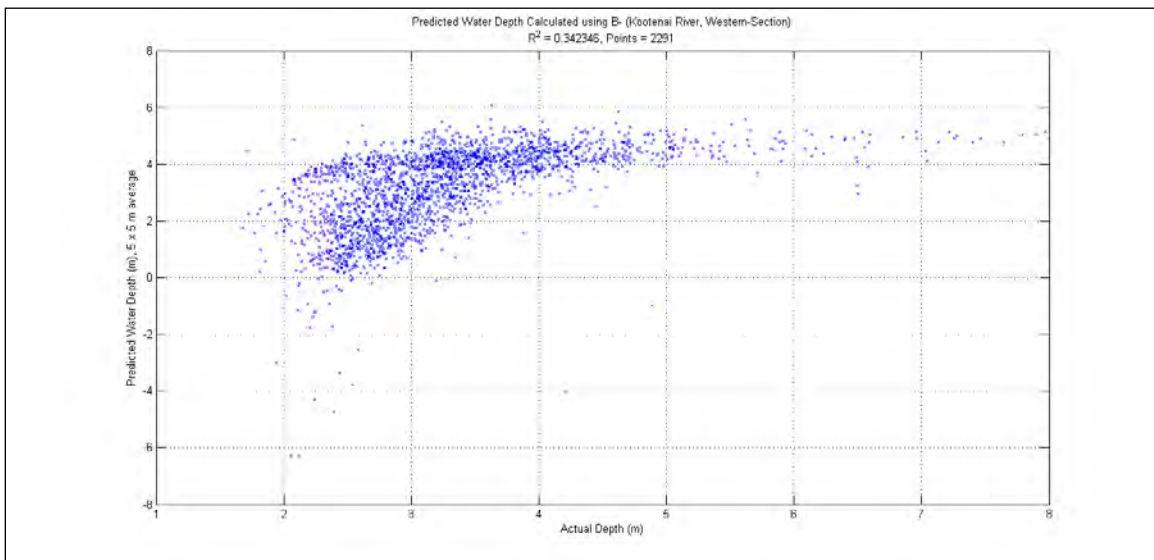


Figure 22. *PWD* Calculated using *Blue*. Beer's Law, Kootenai River, Western Section

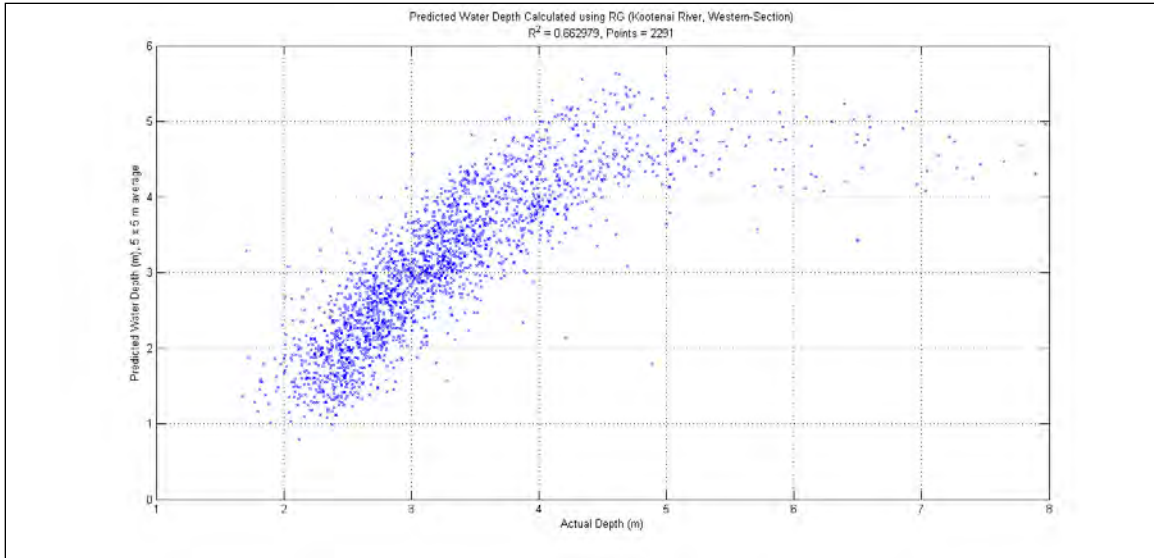


Figure 23. *PWD* Calculated using *Red/Green*. Beer's Law, Kootenai River, Western Section

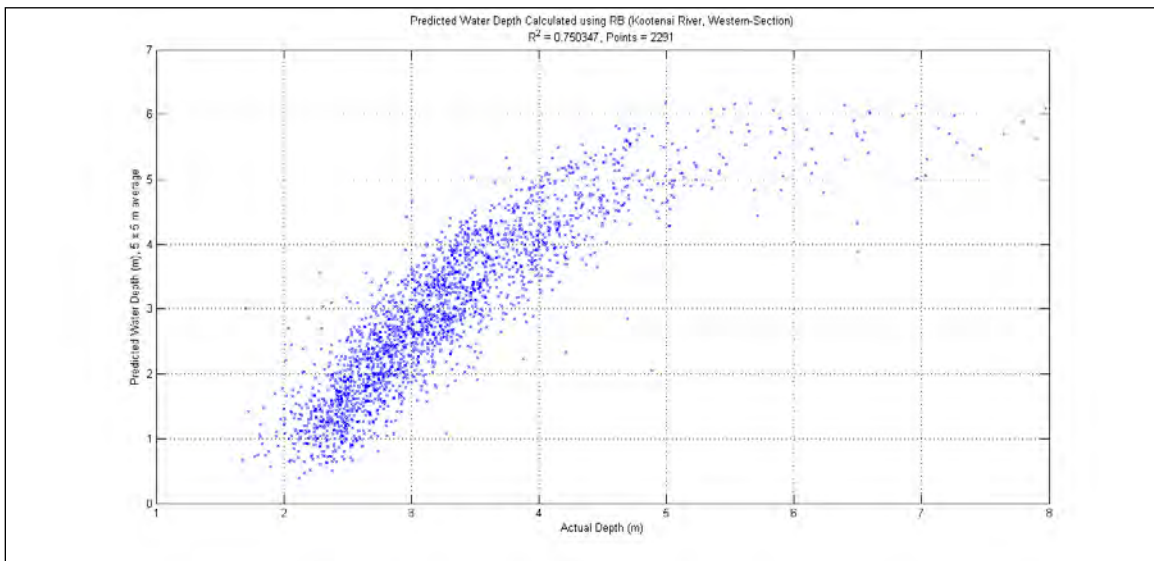


Figure 24. *PWD* Calculated using *Red/Blue*. Beer's Law, Kootenai River, Western Section

## 2. Trinity River

### a. *Sheridan Bar*

Table 4 shows  $R^2$  values for *PWD* using Beer's Law for Sheridan Bar on the Trinity River. It is apparent that the same method that did so well on the Kootenai

River did not do as well on this section of the Trinity River.  $R^2$  values for *Green* and *Blue* are so poor, that they will not even be examined. With  $R^2 = 0.233$  at 2.5 ft radius, *Red* does better than *Green* and *Blue*, but still not very well. The two ratios have the highest  $R^2$  values, with *Red/Green* doing the best overall at 2.5 ft.

Table 4. Beer's Law  $R^2$  Values, Trinity River, Sheridan Bar

	D = 0.5 ft N = 55291	D = 1 ft N = 55479	D = 2.5 ft N = 56254	D = 5 ft N = 57590
Red	0.211	0.224	0.233	0.227
Green	0.021	0.027	0.030	0.028
Blue	0.004	0.005	0.009	0.010
Red/Green	0.383	0.425	0.458	0.453
Red/Blue	0.215	0.264	0.312	0.304

For *Red/Green* (Figure 25), within the 56,000+ points used to calculate depths, there appears to be a defined line correlating *PWD* to actual depths, except for the portion circled in red. Upon closer examination, *PWD* are greatly underestimated, with 1.8 ft being predicted where depth should be closer to 5 ft. *Red/Blue* does not do as well as *Red/Green*, and seems to have a wider spread of values corresponding to an actual depth of about 3 ft, which is also circled in red (Figure 26).

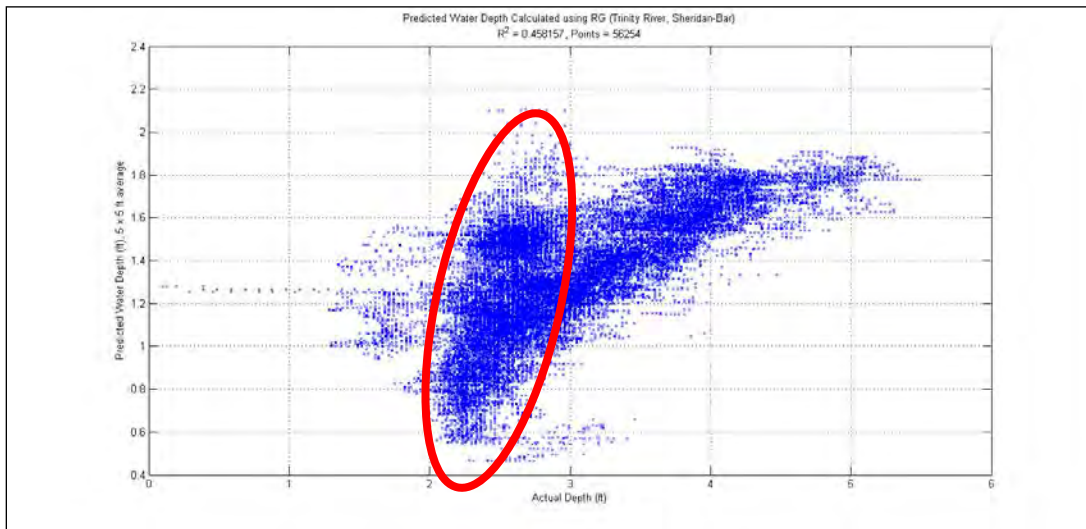


Figure 25. *PWD* Calculated using *Red/Green*. Beer's Law, Trinity River, Sheridan Bar

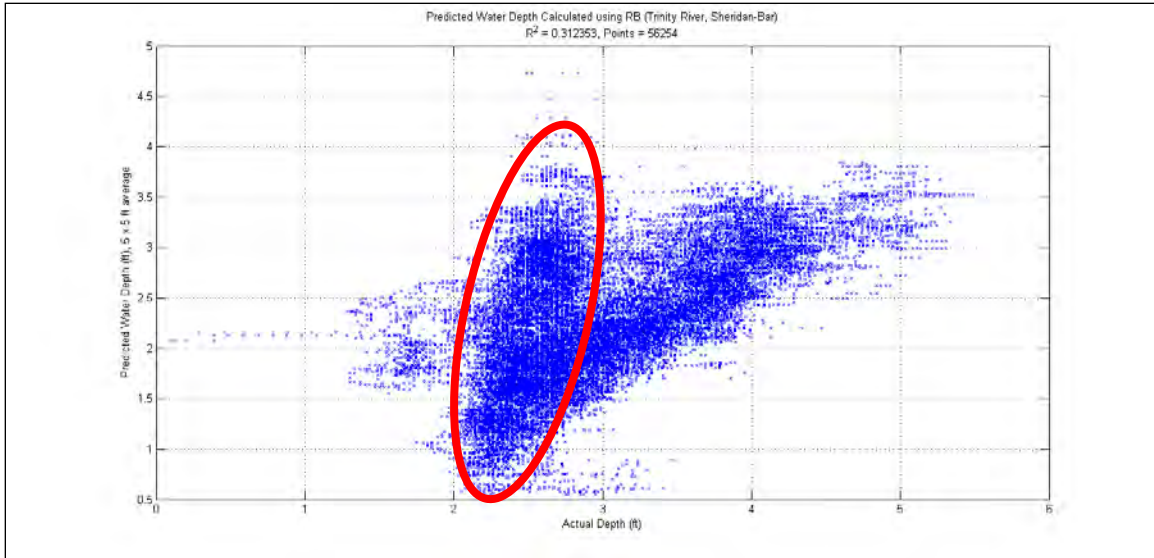


Figure 26. *PWD* Calculated using *Red/Blue* in Beer’s Law, Trinity River, Sheridan Bar

**b. Chapman Ranch**

Table 5 depicts  $R^2$  values for *PWD* using Beer’s Law in the Chapman Ranch section of the Trinity River. Beer’s Law for this section of the river, like Sheridan Bar, did not correlate well, especially when compared to the results from the Kootenai River.  $R^2$  values for *Green* and *Blue* did better than in the Sheridan Bar, but still not well enough to be noteworthy. At a radius of 5 ft, *PWD* using *Red*, *Red/Green*, and *Red/Blue* did the best, with *Red/Green* having the highest  $R^2$  value.

Table 5. Beer’s Law  $R^2$  Values, Trinity River, Chapman Ranch

	D = 0.5 ft N = 55291	D = 1 ft N = 55479	D = 2.5 ft N = 56254	D = 5 ft N = 57590
Red	0.245	0.260	0.291	0.336
Green	0.113	0.128	0.143	0.152
Blue	0.036	0.043	0.051	0.054
Red/Green	0.301	0.324	0.368	0.449
Red/Blue	0.267	0.303	0.358	0.437

Deeper than 5 ft, none of the bands or ratios does well and calculating *PWD* a highly correlated depth. When gathering depths and pixel values for LUT, it was found that beyond this depth, there was very little variation in *DN* for each band. At depths shallower than 5 ft, all three bands with the highest  $R^2$  have a fairly large spread, making it difficult to see any real correlation between actual depth and *PWD*.

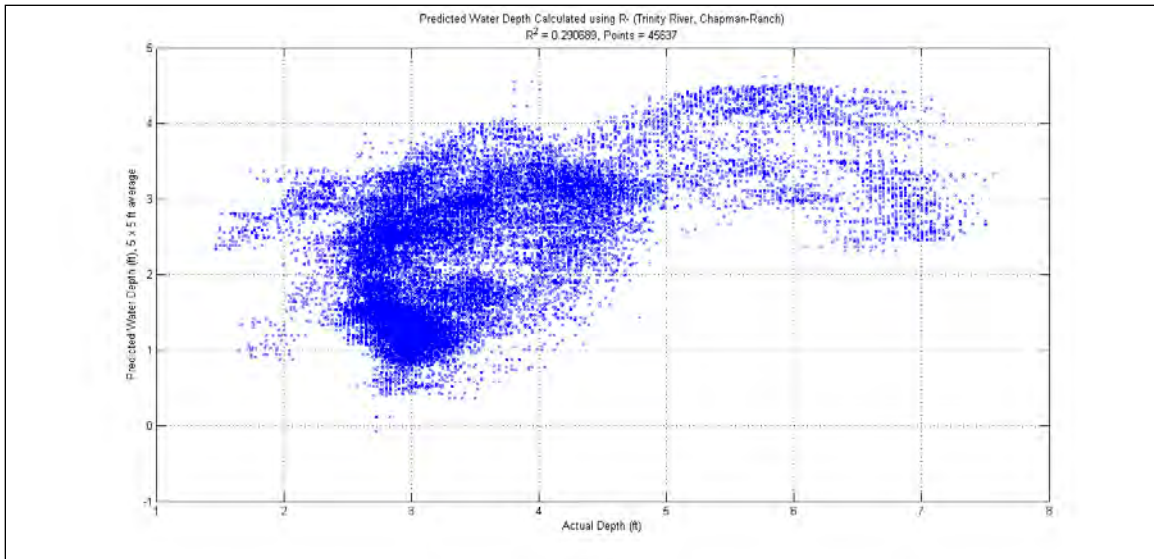


Figure 27. *PWD* Calculated using *Red*. Beer's Law, Trinity River, Chapman Ranch

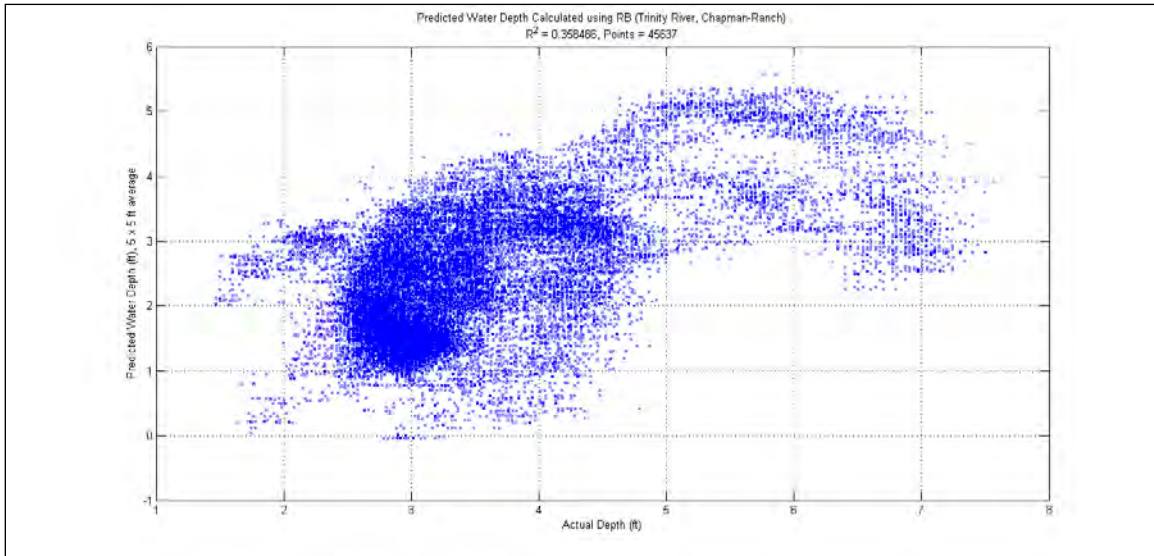


Figure 28. *PWD* Calculated using *Red/Blue*. Beer's Law, Trinity River, Chapman Ranch

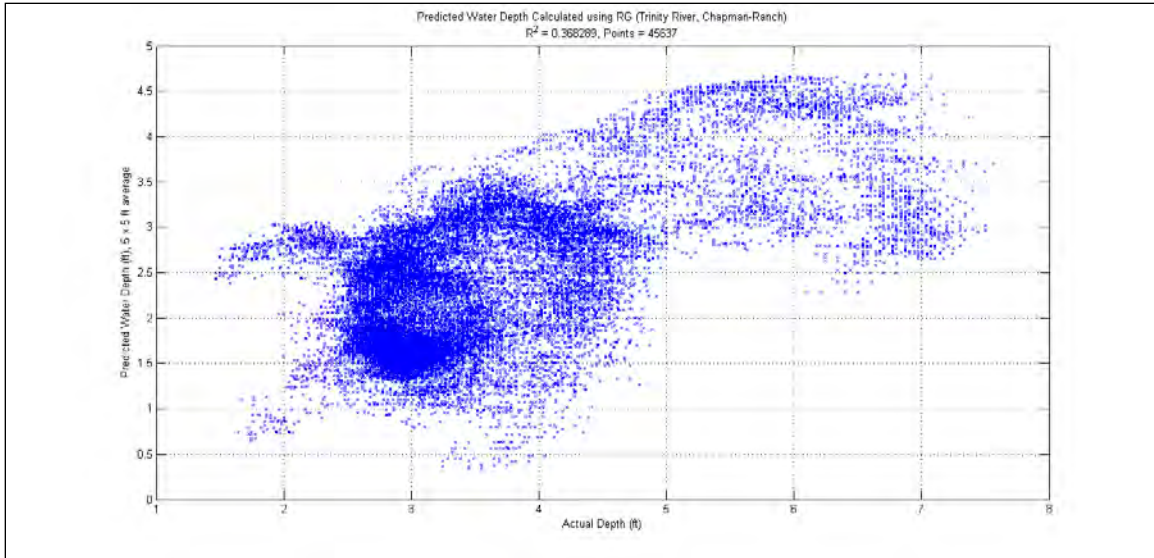


Figure 29. *PWD* Calculated using *Red/Green* in Beer’s Law, Trinity River, Chapman

**B. LOOKUP TABLE VIA POLYNOMIAL REGRESSION**

**1. Kootenai River**

*a. Central Section*

Table 6 shows  $R^2$  values for lookup depths using polynomial regression on the Central Section of the Kootenai River. At a radius of 1 m, *Red* and *Blue* had outliers causing  $R^2$  to decrease drastically, especially when compared to the  $R^2$  value for the ratio of the two bands. For all radii, *Red/Blue* had the highest correlation to actual depth, but was maximum at 2.5 m, a value that is higher than any radius using Beer’s Law method. For comparison, a radius of 2.5 m will be used.

Table 6. LUT  $R^2$  Values, Kootenai River, Central Section

	D = 1 m N = 837	D = 2.5 m N = 868	D = 5 m N = 921	D = 7.5 m N = 961
Red	0.391	0.869	0.893	0.885
Green	0.813	0.878	0.874	0.879
Blue	0.276	0.728	0.758	0.769
Red/Green	0.814	0.875	0.888	0.883
Red/Blue	0.875	0.917	0.912	0.904

Color band *Blue* once again proves to have the lowest correlation on its own. In shallow waters, high variations in *DN* values cause variations in depth, but in deeper waters, variations are less, as seen in Figure 30. *Red*, Figure 31, has the next lowest correlation, which is still high at 0.869. Data points are grouped very close together, but in shallow waters, high *DN* values for *Red* cause negative depths to be predicted. Both *Green* and *Red/Green*, Figures 32 and 33, respectively, have close  $R^2$  values, with *Green* showing spread in shallow waters due to variation in *DN* values, and *Red/Green* showing more of a spread in deeper waters. Finally, *Red/Blue*, which has the highest correlation, has tight grouping for all depths, with very few outliers.

Lookup depths for all bands are close to the actual depths, with very little under prediction as was seen in Beer's Law calculations. *Red/Blue*, Figure 34, is under predicted by about 0.5 m for all depths, where single bands are fairly close to actual depth in deeper waters, but under predict in shallow waters.

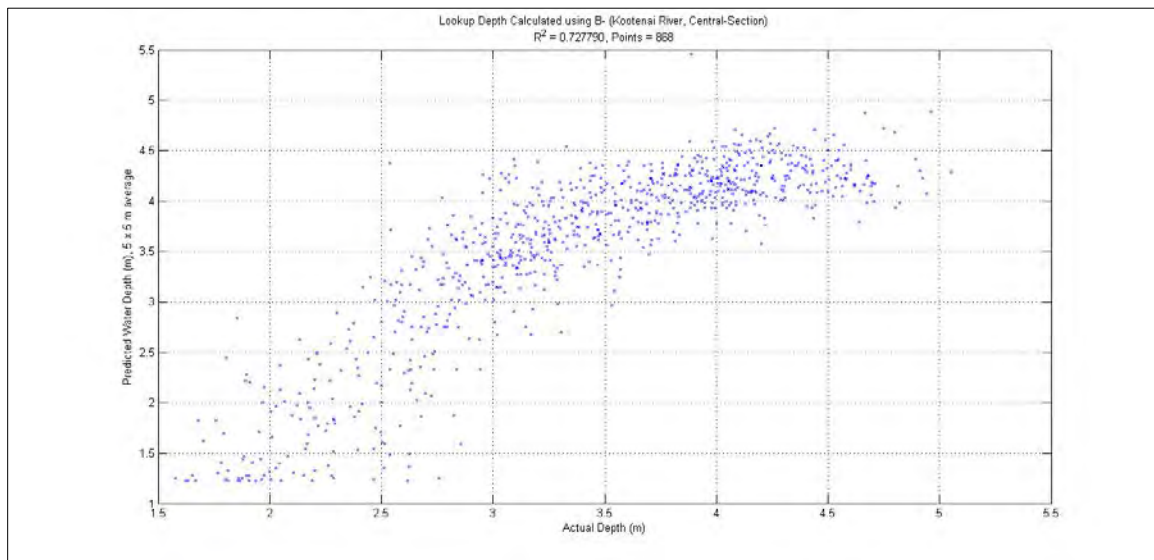


Figure 30. Lookup Depth using *Blue*. Kootenai River, Central Section.

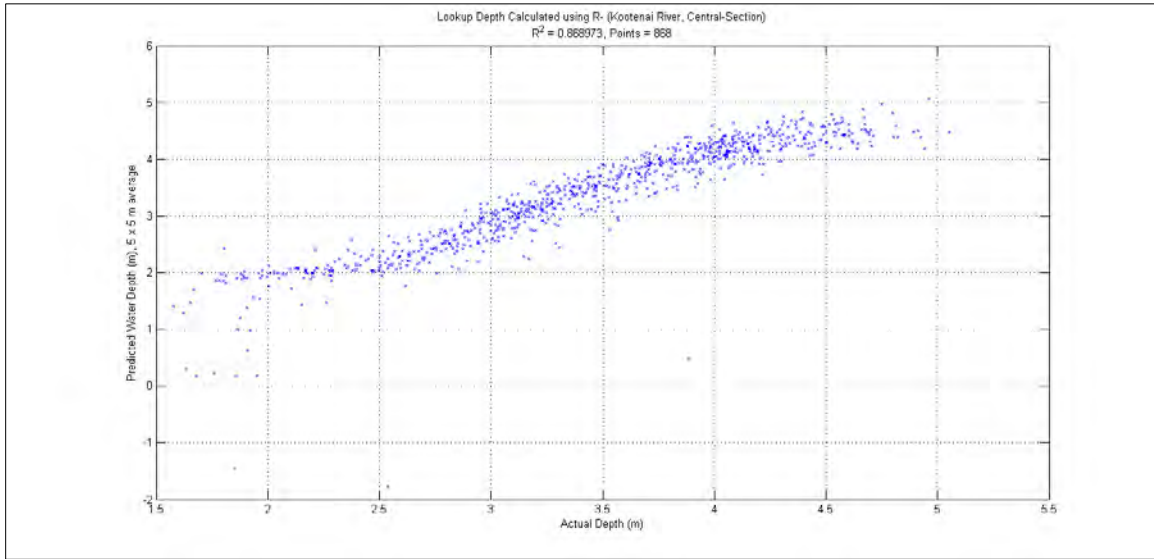


Figure 31. Lookup Depth using *Red*. Kootenai River, Central Section

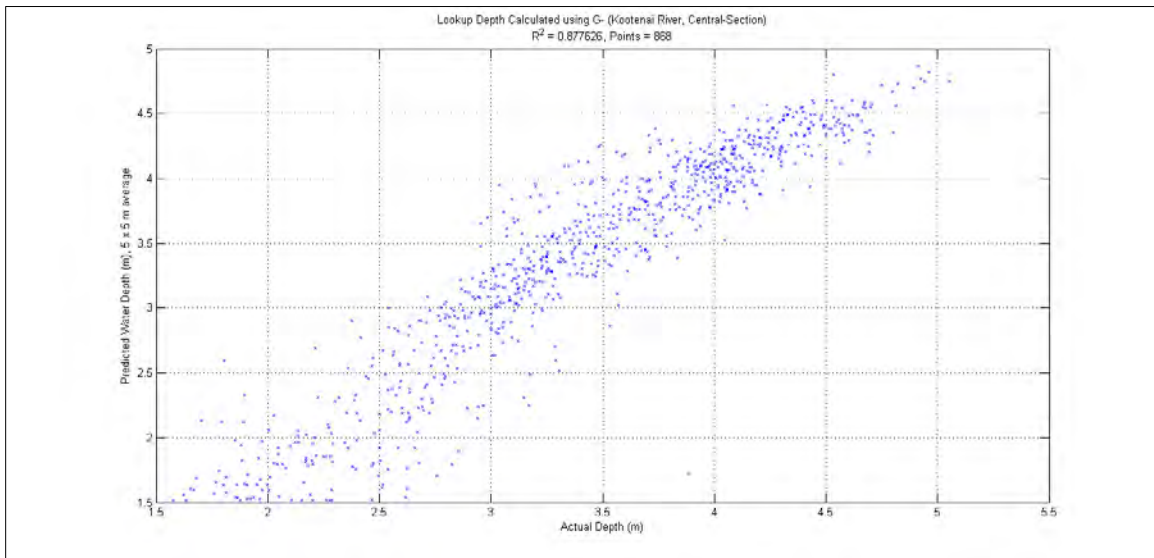


Figure 32. Lookup Depth using *Green*. Kootenai River, Central Section

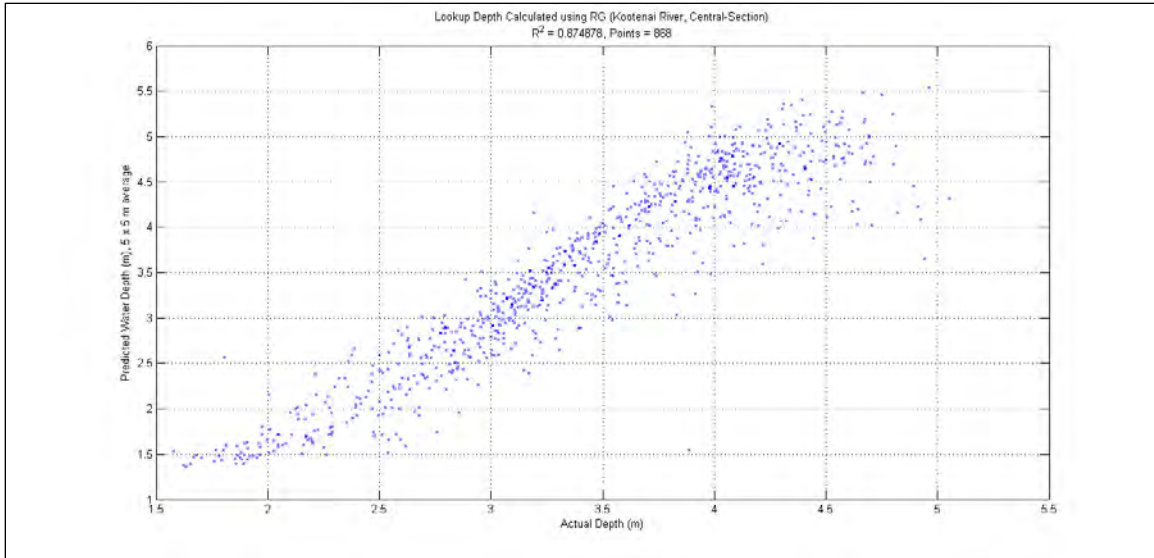


Figure 33. Lookup Depth using *Red/Green*. Kootenai River, Central Section

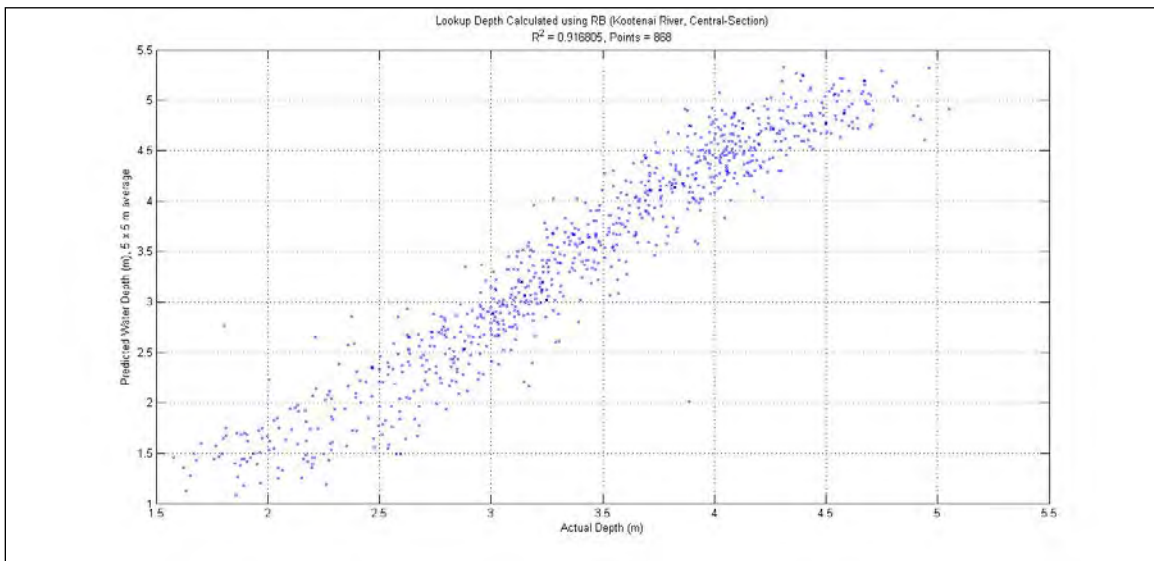


Figure 34. Lookup Depth using *Red/Blue*. Kootenai River, Central Section

***b. Eastern Section***

For the Eastern Section of the Kootenai River, Table 7 shows  $R^2$  values using LUT. Once again in the Eastern Section,  $R^2$  values are much lower than those found in the previous section, with *Green* having the highest correlation. *Red* and *Red/Blue* did well, while *Blue* and *Red/Green* had the lowest correlations.

Table 7. LUT  $R^2$  Values, Kootenai River, Eastern Section

	D = 1 m N = 562	D = 2.5 m N = 598	D = 5 m N = 638	D = 7.5 m N = 674
Red	0.412	0.414	0.419	0.449
Green	0.529	0.532	0.538	0.562
Blue	0.290	0.311	0.320	0.344
Red/Green	0.183	0.220	0.236	0.267
Red/Blue	0.386	0.423	0.433	0.467

None of the bands, or ratios, does very well at actual depths beyond 6 m, as was expected. Removing deeper values from the  $R^2$  calculations would most likely produce higher correlation values, and will be examined in Chapter V.

In Figure 35, *Green* has a large spread of predicted depths in shallow water. *Red*, Figure 36, which has a tighter grouping in shallow waters, still predicts negative depth values due to high *DN*. Although *Green* has the highest correlation, comparing plots shows that *Red/Blue*, Figure 37, actually does the best at predicting water depths. Grouping in shallow waters, less than 6 m, is closer than in the other two plots. Beyond 6 m, there is a larger spread, but this was expected. Lookup depths are slightly under-predicted, approximately 0.5 m, in shallow waters, but appear to be fairly close in deeper waters.

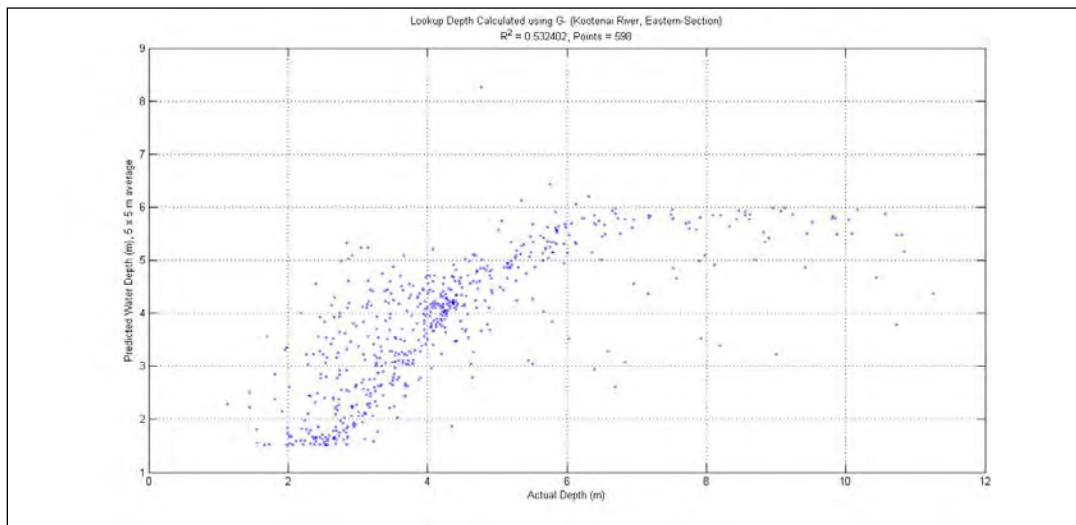


Figure 35. Lookup Depth using *Green*. Kootenai River, Eastern Section

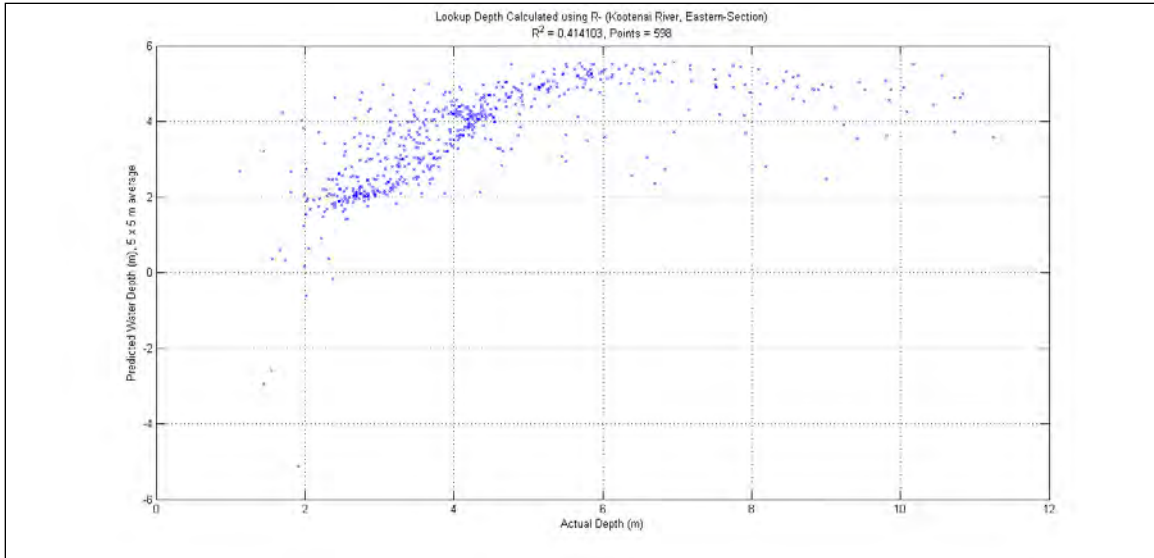


Figure 36. Lookup Depth using *Red*. Kootenai River, Eastern Section

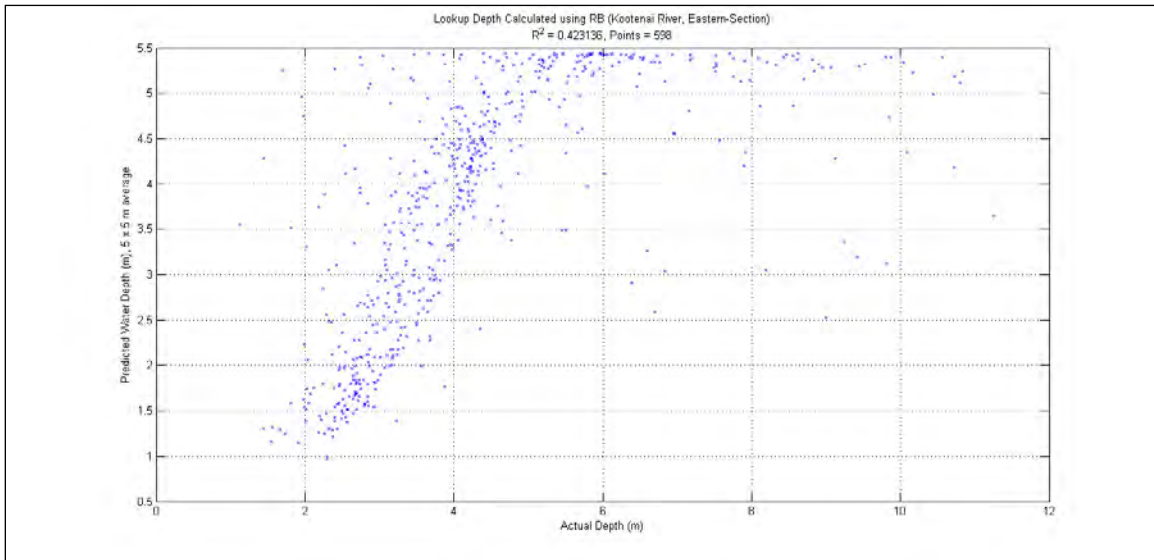


Figure 37. Lookup Depth using *Red/Blue*. Kootenai River, Eastern Section

**c. Western Section**

For the largest section of the Kootenai River, the Western Section, Table 8 shows  $R^2$  values for lookup depths. Single bands, *Red*, *Green*, and *Blue*, did very poorly in this section of the river. For these three bands in the varying radii, high and low *DN* values cause under and over predicted depths, and thus poor  $R^2$  values. However, ratios

of these bands do a much better job of correcting for these high and low *DN* values. The ratios of *Red/Green* and *Red/Blue* do well at all radii, with highest correlations at 2.5 m.

Table 8. LUT  $R^2$  Values, Kootenai River, Western Section

	D = 1 m N = 2194	D = 2.5 m N = 2291	D = 5 m N = 2435	D = 7.5 m N = 2606
Red	0.007	0.006	0.006	0.008
Green	0.039	0.057	0.112	0.198
Blue	0.000	0.000	0.001	0.004
Red/Green	0.669	0.685	0.683	0.655
Red/Blue	0.751	0.762	0.761	0.731

It is possible, and very likely, that if one were to exclude depths greater than 6 m,  $R^2$  values for both ratios would be much higher. Plots of lookup depths for *Red/Green* and *Red/Blue*, Figures 38 and 39 respectively, show tight grouping in shallower waters. Lookup depths for *Red/Green* spread out beyond 3 m, whereas *Red/Blue* remain closely grouped out to 5 m, where ground-truth points become sparse. Beyond 6 m, lookup depths for *Red/Green* vary quite a bit, whereas for *Red/Blue*, they remain predominately within the 5–5.5 m range. In shallow waters, lookup depths for *Red/Green* and *Red/Blue* are under predicted by approximately 1 m, but are fairly close in deeper waters.

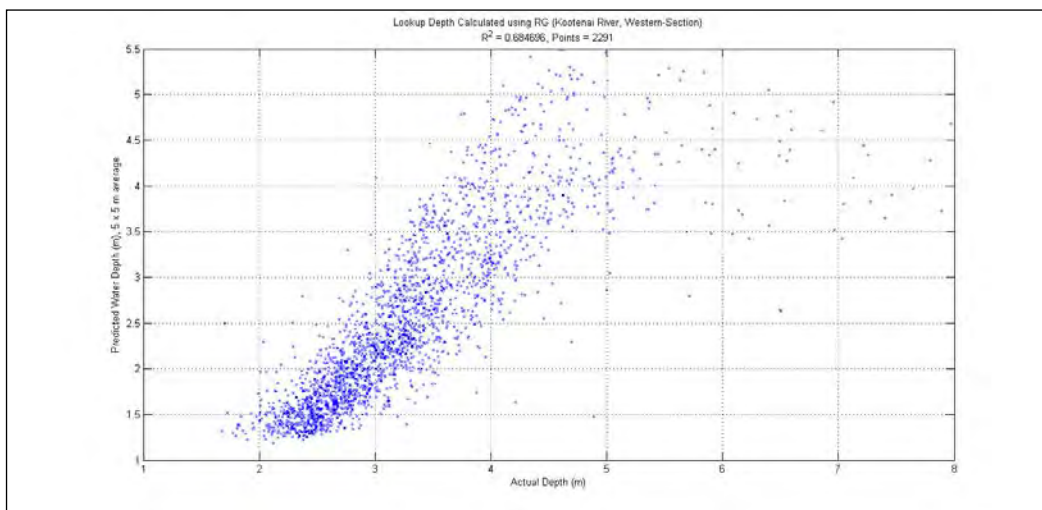


Figure 38. Lookup Depth using *Red/Green*. Kootenai River, Western Section

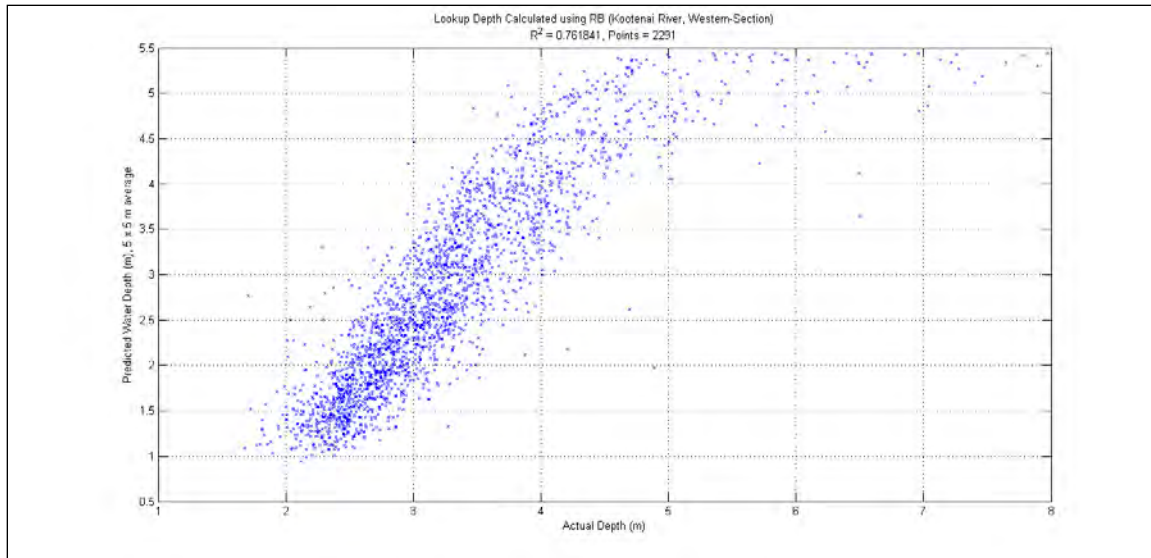


Figure 39. Lookup Depth using *Red/Blue*. Kootenai River, Western Section

## 2. Trinity River

### a. *Sheridan Bar*

Moving to the Trinity River, Table 9 shows  $R^2$  values for lookup depth in the Sheridan Bar section. Correlations between lookup depths and actual depths were not nearly as high as they were for sections in the Kootenai River. At the 2.5 ft radius, *Red/Green* has the highest  $R^2$  value and *Red/Blue* the second highest. The single bands, once again, did poorly in this section of the river.

Table 9. LUT  $R^2$  Values, Trinity River, Sheridan Bar

	D = 0.5 ft N = 55291	D = 1 ft N = 55479	D = 2.5 ft N = 56254	D = 5 ft N = 57590
Red	0.211	0.223	0.232	0.224
Green	0.001	0.005	0.007	0.005
Blue	0.001	0.003	0.023	0.043
Red/Green	0.410	0.458	0.498	0.490
Red/Blue	0.194	0.260	0.317	0.317

Lookup depths for *Red/Green* and *Red/Blue*, Figures 40 and 41, respectively, have a large spread of lookup depths for actual depths at the 2.5–3 ft range, which are circled in red. This signifies that there is a large variation in *DN* values for all three color bands at this depth. Removing this spread of values at 2.5–3 ft and examining the rest of the plots, there appears to be strong correlation between lookup depths and actual depths for both ratios. The majority of lookup depths within this stronger correlation are fairly close to actual depths, with very little under or over prediction.

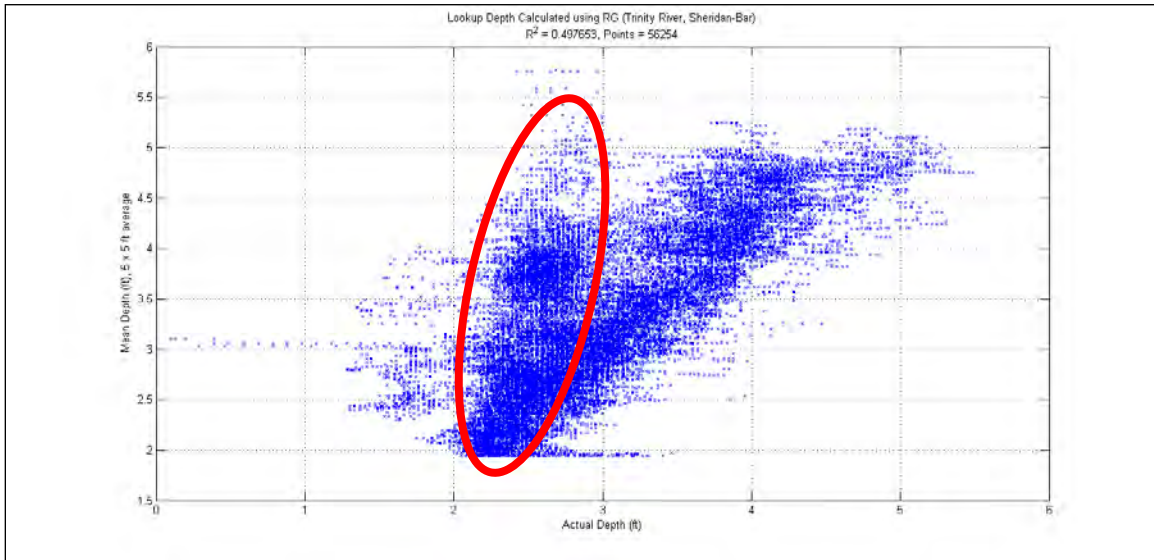


Figure 40. Lookup Depth using *Red/Green*. Trinity River, Sheridan Bar

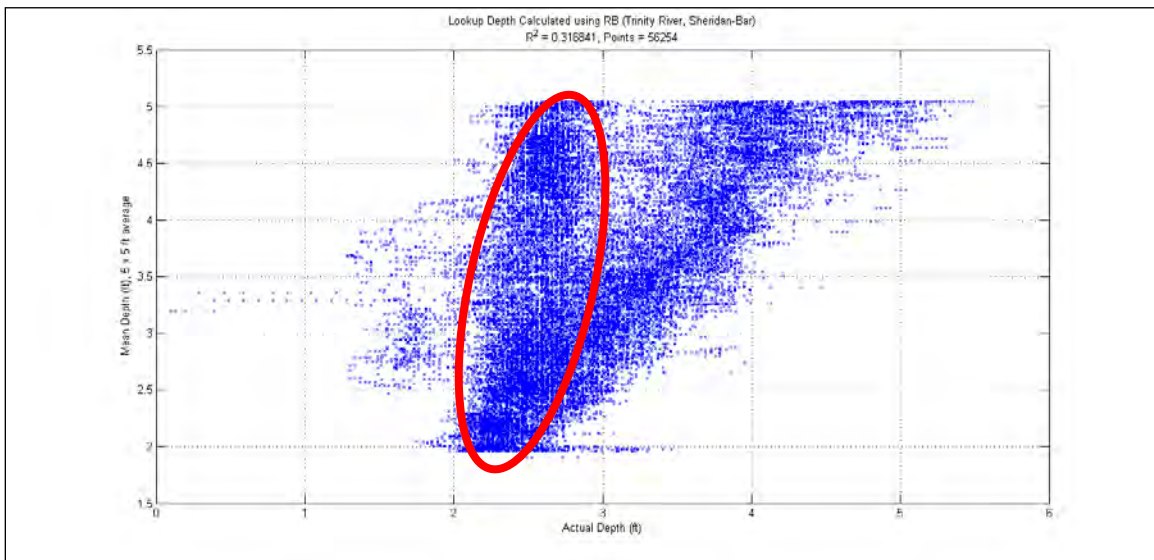


Figure 41. Lookup Depth using *Red/Blue*, Trinity River, Sheridan Bar

**b. Chapman Ranch**

Table 10 shows  $R^2$  values using LUT method for the Chapman Ranch portion on the Trinity River. Correlation between lookup depth and actual depth is poor for all bands and radii. The highest  $R^2$  value occurs for *Red/Blue* at a radius of 5 ft, but even this is poor at 0.335.

Table 10. LUT  $R^2$  Values, Trinity River, Chapman Ranch

	D = 0.5 ft N = 55291	D = 1 ft N = 55479	D = 2.5 ft N = 56254	D = 5 ft N = 57590
Red	0.018	0.025	0.036	0.067
Green	0.003	0.024	0.061	0.087
Blue	0.003	0.015	0.047	0.075
Red/Green	0.032	0.033	0.041	0.057
Red/Blue	0.044	0.121	0.217	0.335

Large variations in  $DN$  at similar depths cause large spread of lookup depths compared to ground-truth data, as shown in Figure 42. Even if one were to remove actual depths greater than 5 ft for calculating  $R^2$ , the spread in values in shallower waters would cause correlation to be poor for this section of the river.

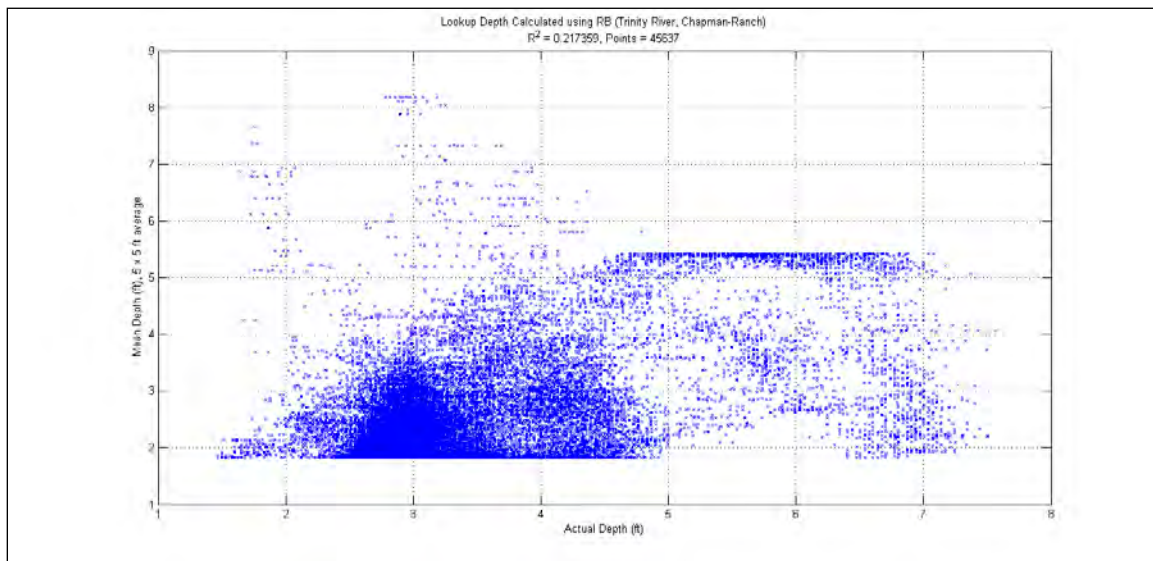


Figure 42. Lookup Depth using *Red/Blue*. Trinity River, Chapman Ranch

## V. DISCUSSION

### A. BEER'S LAW

Previous research has already shown that using Beer's Law to predict water depths from  $DN$  is feasible, but focused on the *Red* color band. It was suggested that using a ratio of color bands would account for differing albedos due to a variation in bottom types (Stumpf et al., 2003; Fonstad and Marcus, 2005; Lyzenga, 1978). As seen in all three sections of the Kootenai River, using only the *Red* band for depth derivations did well, but the ratio of *Red/Blue* did consistently better. There was an issue in the Eastern section of the Kootenai where actual water depths exceeded the depth at which  $DN$  values changed with depth. In this section, *Green* had the highest  $R^2$  value, with *Red/Blue* close behind. Removing the depths at which  $DN$  values no longer change (6 m) and recalculating shows that  $R^2$  for both increases, but *Red/Blue* has a larger increase than *Green* and does a better job of predicting depths closer to the actual depth. *Red* has the highest  $R^2$  value for all radii, but does not calculate depth as closely to actual depths as *Red/Blue*.

Table 11. Beer's Law  $R^2$  Values, Kootenai River, Eastern Section

	D = 1 m N = 480	D = 2.5 m N = 511	D = 5 m N = 547	D = 7.5 m N = 581
Red	0.618	0.656	0.637	0.653
Green	0.537	0.586	0.590	0.605
Blue	0.447	0.493	0.476	0.489
Red/Green	0.485	0.565	0.574	0.599
Red/Blue	0.574	0.639	0.624	0.649

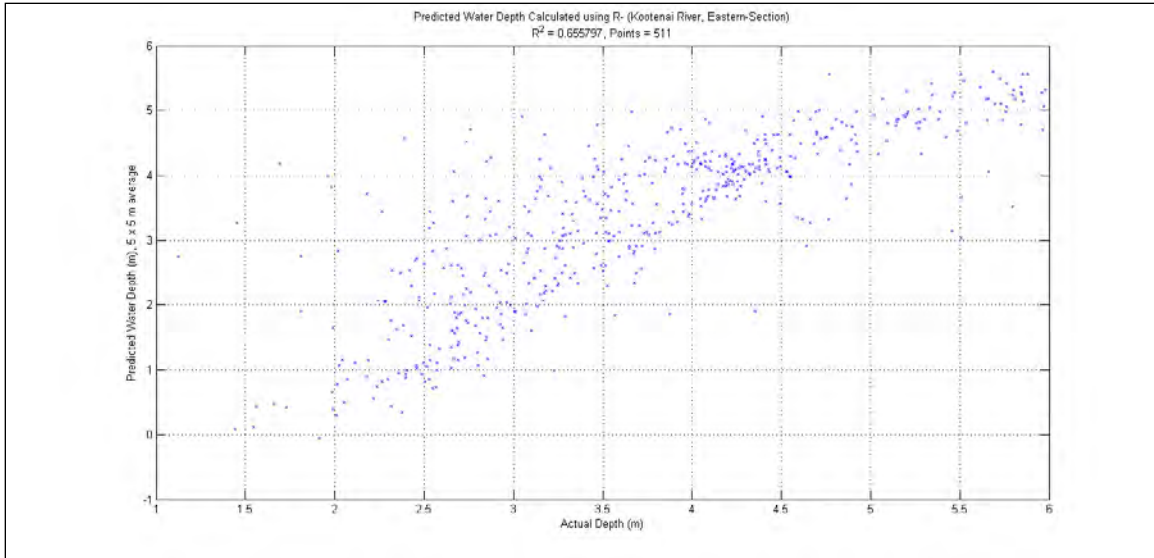


Figure 43. Calculated using *Red*. Beer's Law, Kootenai River, Eastern Section

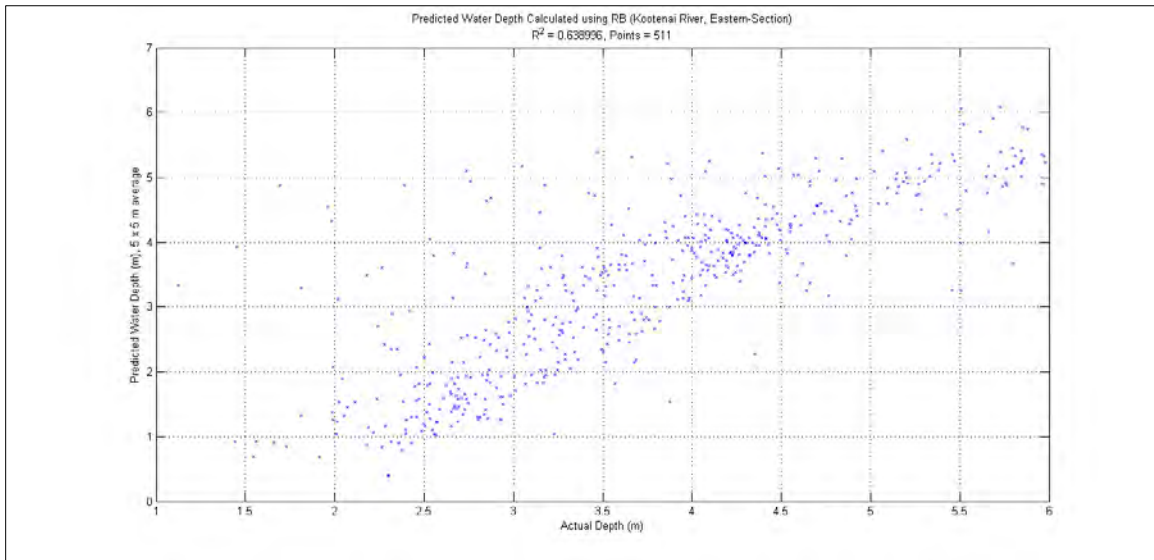


Figure 44. Calculated using *Red/Blue* in Beer's Law, Kootenai River, Eastern Section

For the Trinity River, calculating *PWD* with Beer's Law did not fare as well. For both sections of the river, the single color bands, *Red*, *Green*, and *Blue*, did extremely poorly. The two ratios fared much better, but still did not do well. Looking at Figures 25 and 26 for the ratios in Sheridan Bar, there appears to be some correlation but at an actual depth of 2.5 to 3 ft, there is a wide spread of *PWD* values (portion circled in red). This is

due to a large variation  $DN$  values in each band at the same water depth. Upon closer examination of the imagery, it can be seen that some areas which are still visible from the aircraft are darker than surrounding areas. It is possible that shading from the banks, such as in the northern and southern section of the river, is preventing the same amount of incident light from interacting with the water surface as seen in the central section of the river, where Beer's Law in-situ measurements were acquired.

Selecting a new ROI of just the central section of the river supports this theory. Recalculating depths and  $R^2$  values shows that Beer's Law does work for this river, as seen in Figure 45, but changes in lighting due to sun angle and shading in the scene can cause drastic changes in the calculations.  $R^2$  values for all radii and all bands can be seen in Table 12, which shows *Red* and *Red/Green* having the highest correlations, but both suffer from a severe under-prediction of depths, unlike *Red/Blue*.

Table 12. Beer's Law  $R^2$  Values, Trinity River, Sheridan Bar

	D = 0.5 ft N = 27324	D = 1 ft N = 27558	D = 2.5 ft N = 27975	D = 5 ft N = 28179
Red	0.690	0.741	0.795	0.831
Green	0.332	0.467	0.602	0.670
Blue	0.111	0.164	0.239	0.283
Red/Green	0.685	0.753	0.820	0.844
Red/Blue	0.504	0.628	0.772	0.814

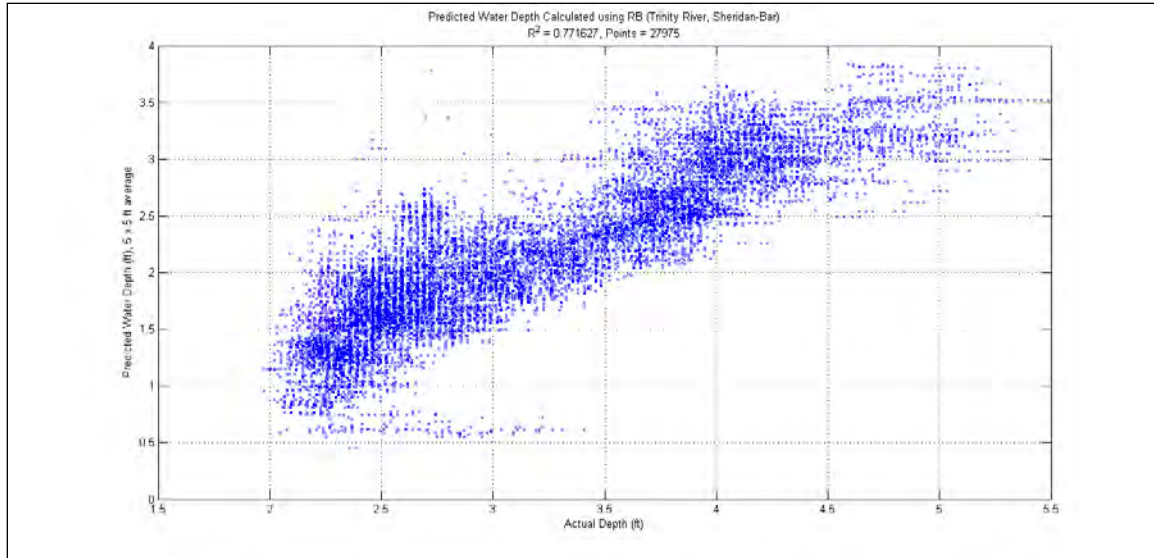


Figure 45. Calculated using *Red/Blue*. Beer's Law, Trinity River, Sheridan Bar

The ratio method introduced by Lyzenga (1978) and Stumpf et al. (2003), which states that changes in bottom albedo affect reflectance for each band similarly, does account for this change in lighting somewhat. Comparing  $R^2$  values for single bands to that for the ratios shows that the ratios do much better when incorporating the entire scene, but still have issues when lighting is not the same for the entire scene.

Similar issues with lighting were observed in the Chapman Ranch section of the Trinity River. Locations with the same depth had pixels with different  $DN$  values. It is not known if the images were taken on the same day at different times, different days at the same time, or different days at different times, so the location of the sun in relation to the aircraft is not known. What can be seen from the images is the relation of the sun to the river. In the Sheridan Bar section, the sun is parallel to the river, where as in the Chapman Ranch section, the sun is perpendicular to the river. It is possible that the orientation of the sun with relation to the river is causing this method to work in some cases and not in others. Water reflectance is partly a function of solar zenith angle, and variations in this solar angle could produce changes in reflectance unrelated to water properties (Novo et al., 1989). For Kootenai river, where this method does work, examining the shadows cast by trees shows the sun is also perpendicular to the river. However, the sensor is much higher, the river much wider, and the banks have less

foliage covering them. From the metadata associated with the imagery, the image was taken just after noon, so the sun was high in the sky, increasing the amount of illumination cast on the river.

Another issue observed in all the data was the continuous under-prediction of water depths using Beer's Law. Some bands fared better, only being off by 0.5 m for Kootenai River, or 0.5 ft for Trinity River, but others did worse with differences closer to 1–1.5 m and 1–1.5 ft, respectively. There are a few different factors that may be causing this, either by themselves or a combination of two or more.

First, when examining the ground-truth data and comparing it to the imagery, it was found that locations having shallow depths in the ground-truth appeared to be dry river bank in the imagery. With both test locations for these rivers being downstream from dams, it is possible that if imagery and ground-truth data were not collected at the same time, changes in dam outflow could change river height in the matter of days.

A second issue is more spectrally based and has to do with the extinction coefficient ( $c(\lambda)$ ). Legleiter et al. (2008) found that for deeper water, in the river environment deep water is greater than 0.4 m (1.3 ft), a low  $c(\lambda)$  causes under-prediction of depths. Legleiter states that the absorption reduces the amount of radiance reflected off the bottom, allowing the contribution from the water column to be greater, making pixel appear brighter to the sensor, and thus shallower when using Beer's Law to calculate depths. A final issue that could be contributing to the under-prediction of depths for both rivers is the bottom type. Again, Legleiter et al. (2008) found that for deeper waters, depths greater than 0.4 m, lower reflectance of a gravel bottom is mistaken for reduced column reflectance due to a shallower depth.

## **B. LUT VIA POLYNOMIAL REGRESSION**

Calculating depths using polynomial regression worked much better than was initially anticipated. From the Central Section of the Kootenai River, depths from the lookup table for *Red/Blue* at a radius of 2.5 m did better than the more widely used method of Beer's Law for all the bands. Single color bands, *Red*, *Green*, and *Blue*, did well in the Central Section of the Kootenai River, but in other sections had negative water

depths where bright pixels occurred, and on the Trinity River they did extremely poorly. The ratio method for the LUT proved to be the best method, having the highest  $R^2$  values for all the areas, even on the Chapman Ranch section of the Trinity River.

On the Eastern Section of the Kootenai River,  $R^2$  values were low. As was the case in the Beer's Law method, this is due to depths beyond 6 m flattening out where DN values no longer change. Removing these depths, and recalculating  $R^2$  produces much better results, as can be seen in Table 13 and Figure 46. With the removal of these depths, *Red*, on its own, has slightly higher  $R^2$  values than *Red/Blue*, but not by much.

Table 13. LUT  $R^2$  Values, Kootenai River, Eastern Section

	D = 1 m N = 480	D = 2.5 m N = 511	D = 5 m N = 547	D = 7.5 m N = 581
Red	0.585	0.622	0.603	0.622
Green	0.565	0.600	0.585	0.598
Blue	0.443	0.480	0.454	0.470
Red/Green	0.500	0.585	0.576	0.599
Red/Blue	0.549	0.619	0.612	0.635

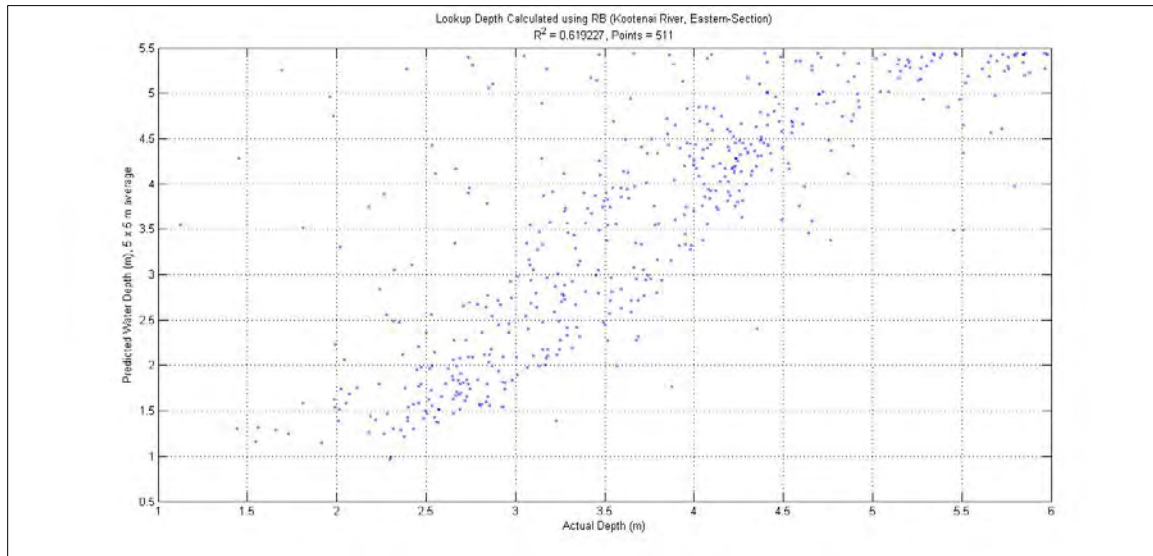


Figure 46. Lookup Depth using *Red/Blue*. Kootenai River, Eastern Section

The same lighting issues that afflicted the Beer's Law method on the Trinity River also affected the LUT method. Removing the sections that had bank shading in the Sheridan Bar section, and focusing on the central portion, produces much better results for all bands, but especially for *Red/Green* (Figure 47), which has a higher  $R^2$  value when compared to the *PWD* using Beer's Law (Figure 45). A smaller section was also chosen for the Chapman Ranch section of the Trinity River, but results were still extremely poor. It is very likely that lighting issues that caused problems with the Beer's Law method in this section of the river also affected the LUT method.

Table 14. LUT  $R^2$  Values, Trinity River, Sheridan Bar

	D = 0.5 ft N = 27324	D = 1 ft N = 27558	D = 2.5 ft N = 27975	D = 5 ft N = 28179
R	0.702	0.753	0.807	0.841
G	0.011	0.097	0.244	0.326
B	0.000	0.001	0.001	0.067
R/G	0.718	0.793	0.864	0.888
R/B	0.484	0.653	0.797	0.846

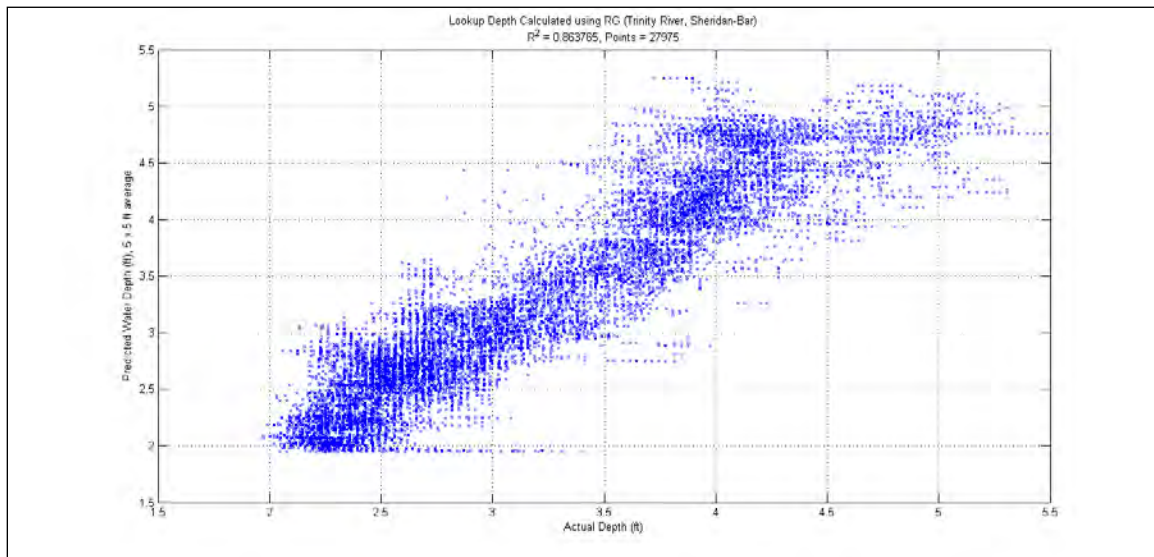


Figure 47. Lookup Depth using *Red/Green*. Trinity River, Sheridan Bar

Throughout most areas, LUT depths are much closer to the actual depths, and don't suffer as much from under-prediction due to water column properties, as seen in Figure 34. The most likely explanation for this is that using multiple depths, relating them to pixel values, and creating a lookup table via polynomial regression tunes pixel values to depths. As seen in Figure 9, the curve for the LUT method in the central section of the Kootenai River follows the actual *DN* values much closer than the exponential curve plotted using Beer's Law. The Beer's Law method depends on the extinction coefficient being constant for the entire river, whereas the using multiple depths to create a third order polynomial continually resets the depths to pixel values at a given depth.

The LUT method isn't without its flaws. It doesn't do well when trying to match pixel values, or ratios, to depths that fall outside the bounds used to create it, i.e. deeper than 6 m or shallower than 1.5 m for Kootenai River. In these instances it does tend to under-predict the actual water depth. Fewer known depths and locations would also make using the LUT difficult. With two points, a linear approximation would be made and the exponential curve that occurs would be lost. Three points would possibly catch the curve, but it would depend on if they were collected at the right depths, and would not see if there were any inflection points in the actual attenuation of light in water. More depths that correspond to varying pixel values would be best, especially if a greater number of depths were collected in shallower water that correspond to high attenuation of *Red*, and fewer depths in deeper water where *DN* for all pixels remains near constant. This could likely be accomplished with as few as 5–10 points.

Creating a lookup table for the ratios can be difficult as well. For single color bands, such as *Red*, as depth changes, *DN* values for *Red* change approximately exponentially. Creating a lookup table for this case is much easier since every change in pixel value should correspond to a change in depth. This becomes much more difficult when using a ratio, which had the best results in this research. Different values of *Red* and *Blue* can produce the same ratio. Also, *Blue* does not vary as quickly as *Red*, so there are instances where *Red* changes considerably over depth and *Blue* will vary slightly, if at all. Taking the max and min of each value in a scene and then creating ratios based on a

linear change does not work. This means that to create a lookup table for a ratio, the initial values used to create the third order polynomial should be used. Between each depth point, an even spacing between the ratios can be found that corresponds to the amount of change in depth. For the Kootenai River, this spacing was found to be 0.05, which corresponded to a 0.8–0.9 m change in water depth. An example of this can be seen in Table 15.

Table 15. Lookup Table for Kootenai River

$(R/B)^{-1}$ Value	1.35	1.40	1.45	1.50	1.55	1.60	1.65	1.70	1.75	1.80	1.85	1.90	1.95
Depth (m)	-1.56	-1.64	-1.63	-1.82	-1.91	-1.99	-2.08	-2.17	-2.25	-2.34	-2.42	-2.51	-2.59

THIS PAGE INTENTIONALLY LEFT BLANK

## VI. CONCLUSION

### A. METHODOLOGY

The scope of this thesis was to examine two different methods for deriving water depths from UAV imagery; one method expounded on previous research, and the other attempted a new approach. Each method has its strengths as well as its flaws and limitations.

Previous research has shown the feasibility of using Beer's Law to derive water depths from a river, with a limitation being the use of a single band. Using a ratio of bands, specifically *Red/Blue*, proved to have higher correlation but suffered from an under-prediction of depths. The second method, LUT via polynomial regression, had more in-situ measurements, but didn't rely on radiative transfer fundamentals. A greater number of measurements cause *DN* values, or ratios, to reset at new depths so there is less under-prediction. When compared to the widely used Beer's Law method, it was more accurate, showing that it is a viable alternative. It is limited by where the depth measurements are taken and that these measurements correspond to differing pixel values.

Caution needs to be applied when using these methods, and it needs to be remembered that these methods are river and event specific (Westaway et al., 2003). Equations or tables created for the Kootenai River will not work on another river. As seen on the Trinity River, two different locations had completely different results, possibly due to sun azimuth with relation to the river.

### B. OPERATIONAL FEASIBILITY

Either of these methods are viable options for use in the field. Beer's Law method has more assumptions, and can greatly under-predict depths unless corrections are made. Using the LUT requires more measurements, but in the end could prove to be the more viable option for field use, since it is as accurate, if not more, and easier to use.

For example, using a small UAV, a team could fly a route over a river when the sun angle produces the greatest amount of illumination, collecting still images or FMV. From the collected imagery, points can be selected in the immediate vicinity of the ground control station that have a distinct change in color corresponding to a change in depth. Using these locations collected from imagery, the team could collect corresponding river depths with a handheld sonar, tape measure and GPS, or lead line and a control point in the imagery. Other options would be to use points collected from hull mounted fathometers as ground truth, or from disposable buoys, and relating these back to the imagery. These points can then be used as the known depth for Beer's Law, or utilized to calculate coefficients for a third order polynomial and create a LUT. Depending on computing capability in the field, and the method chosen, a chart can be created, similar to the simple one in Figure 48, or a table, like Table 15, that can be quickly used to correlate color to depth.

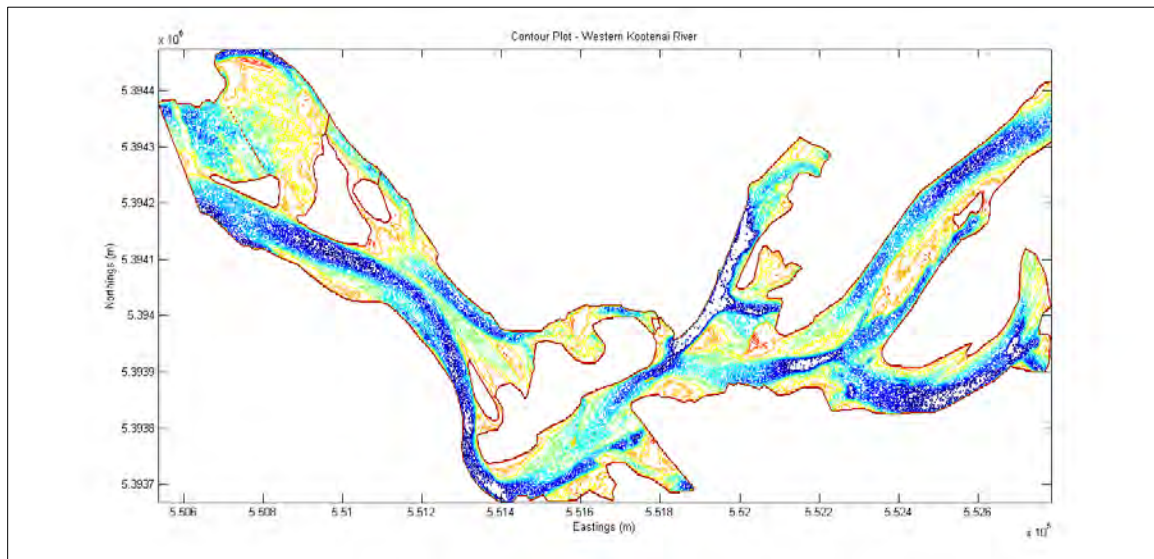


Figure 48. Western Kootenai River Contour Plot, LUT Method

### C. FUTURE RESEARCH

There are opportunities to expound upon this research. The first and foremost is to use actual UAV imagery. This can be high resolution still imagery, or using full motion video (FMV) and video stitching software, such as GeoView, to create an image.

More rivers also need to be examined, though. This research only looked at two rivers, but with more rivers, other factors can be taken into consideration, such as turbidity, sun angle, and bottom type. Another follow on item would be automating the selection of ROIs in ENVI, or some other software tool. Many UAVs have the ability to chose between collecting color imagery, or Thermal-IR. With the Thermal-IR imagery, it is possible to exploit the difference in temperature between wetted areas and dry areas to determine water edge. This can then be applied to the color image to pull out the wetted area.

A final option would be to see the operational relevance of this research. Are the methods, and the collection techniques needed, simple enough to use? These methods were not meant to be used to create models, but to assist in route and mission planning. The question can also be asked, is the data produced good enough for this purpose? To answer these questions, personnel operating in these environments would need access to these tools, utilize them, and determine if the products produced are relevant.

THIS PAGE INTENTIONALLY LEFT BLANK

## LIST OF REFERENCES

- Carbonneau, P. E., Lane, S. N., Bergeron, N., 2006: Feature based image processing methods applied to bathymetric measurements from airborne remote sensing in fluvial environments. *Earth Surface Processes and Landforms*, **31**, 1413–1423.
- Densham, M. P. J., 2005: Bathymetric Mapping with Quickbird data. M. S. Thesis, Dept. of Oceanography, Naval Postgraduate School
- Fonstad, M. A., Marcus, W. A., 2005: Remote sensing of stream depths with hydraulically assisted bathymetry (HAB) models. *Geomorphology*, **72**, 320–339.
- Green, E. P., Mumby, P. J., Edwards, A. J., Clark, C. D., (Ed. A. J. Edwards), 2000: Remote Sensing Handbook for Tropical Coastal Management. *Coastal Management Sourcebook 3*, UNESCO, Paris. x +316 pp.
- Krause, K., 2005. Radiometric Use of QuickBird Imagery. Technical Note, DigitalGlobe, Inc., 18 pp.
- Legleiter, C. J., Roberts, D. A., 2009: A forward image model for passive optical remote sensing of river bathymetry. *Remote Sensing of the Environment*, **113**, 1025–1045.
- Legleiter, C. J., Roberts, D. A., Lawrence, R. L., 2009: Spectrally based remote sensing of river bathymetry. *Earth Surface Processes and Landforms*, **34**, 1039–1059.
- Lejot, J., Delacourt, C., Piégay, H., Fournier, T., Allemand P., 2007: Very high spatial resolution imagery for channel bathymetry and topography from an unmanned mapping controlled platform. *Earth Surfaces and Landforms*, **32**, 1705–1725.
- Lyzenga, David R., 1979: Passive remote sensing techniques for mapping water depth and bottom features. *Applied Optics*, **17**, 379–383.
- Lyzenga, David R., 1981: Remote sensing of bottom reflectance and water attenuation parameters in shallow water using aircraft and Landsat data. *Remote Sensing*, **2**, 71–82.
- Mobley, Curtis D., 1994: *Light and Water: Radiative Transfer in Natural Waters*. Academic Press, Inc., 592 pp.
- Mobley, C. D., and Coauthors, 2005: Interpretation of hyperspectral remote-sensing imagery by spectrum matching and look-up tables. *Applied Optics*, **44**, 3576–3592.

- Novo, E. M. M., Hansom, J. D., Curran, P. J., 1989: The effect of viewing geometry and wavelength on the relationship between reflectance and suspended sediment concentration. *Remote Sensing*, **10**, 1357–1372.
- Philpot, William D., 1989: Bathymetric mapping with passive multispectral imagery. *Applied Optics*, **28**, 1569–1578.
- Russ, John C., 1994: *The Image Processing Handbook*. 2<sup>nd</sup> Edition. CRC Press, Inc., 674 pp.
- Schowengerdt, Robert A., 1997: *Remote Sensing: Models and Methods for Image Processing*. 2nd ed. Academic Press, 522 pp.
- Stumpf, R. A., Holderied, K., Sinclar, M. 2003: Determination of water depth with high-resolution satellite imagery over variable bottom types. *Limnology and Oceanography*, **48**, 1 part 2, 547–556.
- Thomas, Gary E., Stamnes, Knut, 1999: *Radiative Transfer in the Atmosphere and Ocean*. Cambridge University Press, 517 pp.
- Westaway, R. M., Lane, S. N., Hicks, D. M., 2003: Remote sensing of large-scale braided, gravel-bed rivers using digital photogrammetry and image analysis. *International Journal of Remote Sensing*, **24**, 795–815.
- Wikipedia*, s.v., “Kootenai River.” [Available online at [http://en.Wikipedia.org/wiki/Kootenai\\_River](http://en.Wikipedia.org/wiki/Kootenai_River)]
- Wikipedia*, s.v. “Trinity River (California).” [Available online at [http://en.Wikipedia.org/wiki/Trinity\\_River\\_\(California\)](http://en.Wikipedia.org/wiki/Trinity_River_(California))]

## INITIAL DISTRIBUTION LIST

1. Defense Technical Information Center  
Ft. Belvoir, Virginia
2. Dudley Knox Library  
Naval Postgraduate School  
Monterey, California
3. Professor Wendell Nuss  
Department of Meteorology  
Naval Postgraduate School  
Monterey, California
4. Captain (Ret) Jeffrey Kline  
Consortium for Robotics and Unmanned Systems Education and Research  
(CRUSER)  
Naval Postgraduate School  
Monterey, California
5. Commander Robert Witzleb  
Commanding Officer, Naval Oceanography Special Warfare Command  
San Diego, California
6. Ms. Melody Coats  
Director Operational and Tactical Analysis Division, NP21  
Naval Oceanographic Office  
Stennis Space Center, Mississippi